

THE GREATER IMPACT OF MERGERS ON THE GROWTH OF MASSIVE GALAXIES: IMPLICATIONS FOR MASS ASSEMBLY AND EVOLUTION SINCE $Z \simeq 1^*$ KEVIN BUNDY^{1,2}, MASATAKA FUKUGITA³, RICHARD S. ELLIS^{4,5}, THOMAS A. TARGETT⁴, SIRIO BELL⁶, TADAYUKI KODAMA⁷*Submitted to ApJ and revised after referee comments*

ABSTRACT

Using deep infrared observations conducted with the MOIRCS imager on the Subaru Telescope in the northern GOODS field combined with public surveys in GOODS-S, we investigate the dependence on stellar mass, M_* , and galaxy type of the close pair fraction ($5h^{-1}$ kpc $< r_{\text{sep}} < 20h^{-1}$ kpc) and implied merger rate. In terms of combined depth and survey area, our publicly available mass-limited sample represents a significant improvement over earlier infrared surveys used for this purpose. In common with some recent studies we find that the fraction of paired systems that could result in major mergers is low ($\sim 4\%$) and does not increase significantly with redshift to $z \approx 1.2$, with $\propto (1+z)^{1.6 \pm 1.6}$. Our key finding is that massive galaxies with $M_* > 10^{11} M_\odot$ are more likely to host merging companions than less massive systems ($M_* \sim 10^{10} M_\odot$). We find evidence for a higher pair fraction for red, spheroidal hosts compared to blue, late-type systems, in line with expectations based on clustering at small scales. So-called “dry” mergers between early-type galaxies devoid of star formation represent nearly 50% of close pairs with $M_* > 3 \times 10^{10} M_\odot$ at $z \sim 0.5$, but less than 30% at $z \sim 1$. This result can be explained by the increasing abundance of red, early-type galaxies at these masses. We compare the volumetric merger rate of galaxies with different masses to mass-dependent trends in galaxy evolution. Our results reaffirm the conclusion of Bundy et al. (2007) that major mergers do not fully account for the formation of spheroidal galaxies since $z \sim 1$. In terms of mass assembly, major mergers contribute little to galaxy growth below $M_* \sim 3 \times 10^{10} M_\odot$ but play a more significant role among galaxies with $M_* \gtrsim 10^{11} M_\odot$ $\sim 30\%$ of which have undergone mostly dry mergers over the observed redshift range. Overall, the relatively rapid and recent coalescence of high mass galaxies mirrors the expected hierarchical growth of halos and is consistent with recent model predictions, even if the top-down suppression of star formation and morphological evolution (i.e., “downsizing”) involves additional physical processes.

Subject headings: galaxies: evolution — galaxies: formation — galaxies: interactions

1. INTRODUCTION

Recent surveys have challenged the traditional view that merging between dark matter halos governs the mass assembly history and evolution of the galaxies hosted by these halos. The surprising abundance of established massive galaxies at $z \simeq 2$ (e.g., Glazebrook et al. 2004; Cimatti et al. 2004) has been followed by increasing evidence for an early completion of star formation in the most massive galaxies, followed by continued activity in lower-mass systems—a phenomenon now termed “downsizing” (e.g., Juneau et al. 2005; Treu et al. 2005; Bundy et al. 2006; Borch et al. 2006; Cimatti et al. 2006; Bell et al. 2007; Cowie & Barger 2008). These observations reveal top-down evolutionary patterns that stand in contrast to the expected hierarchical, or bottom-up, nature of CDM halo

assembly.

While semi-analytic models employing various energy feedback prescriptions have moved closer to reproducing top-down behavior within the hierarchical framework (Croton et al. 2006; Bower et al. 2006; De Lucia et al. 2006; Cattaneo et al. 2008; Stringer et al. 2008), it has not been observationally possible to verify the CDM prediction that via merging, more massive galaxies are assembled at later times. In principle, the signal is encoded in the evolving stellar mass function (MF) which would be expected to show a rising number density at the high-mass end as a function of cosmic time. Current surveys, however, are too much affected by cosmic variance (or, more accurately, sample variance) uncertainties to confirm this trend (see Stringer et al. 2008). It is also difficult to separate evolution in the MF resulting from galaxy mergers from that associated with star formation (SF) (Drory & Alvarez 2008). The clear alternative is to study galaxy mergers directly and to quantify their role in driving mass assembly by determining how the galaxy merger rate depends on mass.

In addition to driving mass assembly, major mergers (defined here to be those involving components with a mass ratio greater than 1/4) have also been proposed as the key mechanism that transforms disk-like galaxies into spheroidals (Toomre 1977). It may also shut off star formation via triggered AGN feedback (see Hopkins et al. 2007). Mergers may not only move galaxies onto the “red sequence,” but so-called “dry mergers” between red-sequence systems have been invoked to explain the increasing contribution at $M_* > 10^{10} M_\odot$ to the global stel-

* Based on observations collected at the Subaru Telescope, which is operated by the National Astronomical Observatory of Japan, and with the NASA/ESA HST, obtained at STScI, which is operated by AURA, under NASA contract NAS5-26555.

¹ Reinhardt Fellow, Department of Astronomy, University of Toronto, 60 George Street, Toronto ON M5S 3H8, Canada

² Hubble Fellow, Astronomy Department, University of California, Berkeley, CA 94705

³ Institute for Cosmic Ray Research, University of Tokyo, Kashiwa 2778582, Japan

⁴ Astronomy, Mail Stop 105-24, California Institute of Technology, Pasadena CA 91125

⁵ Department of Astrophysics, Keble Road, Oxford OX1 3RH, UK

⁶ Universitá degli Studi di Bologna, via Ranzani 1, Bologna I-40127, Italy

⁷ National Astronomical Observatory of Japan, Mitaka, Tokyo 181-8588, Japan

lar mass density from red galaxies. (e.g., van Dokkum 2005; Faber et al. 2007; Bell et al. 2007).

The fundamental question is whether the *major* merger rate is high enough to explain the mass-dependent increase in the numbers of spheroidal and red-sequence galaxies or whether other mechanisms for building spheroidal systems are needed. Bundy et al. (2007) appealed to numerical simulations to argue that the predicted major merger rate among dark matter halos is too low. A similar conclusion was also reached by Genel et al. (2008). It is now imperative to compare the formation rate of spheroidals to observations capable of identifying major mergers and resolving their frequency as a function of mass.

Previous observational attempts to measure the galaxy merger rate since $z \sim 1$ have faced a number of challenges and sometimes disagree in their conclusions. The derived rate depends on the assumed efficiency and merger timescale, but more importantly, merger definitions vary among authors. Additionally, it has been difficult to distinguish major from minor mergers. At $z \lesssim 1$, the merger rate has been estimated based on the occurrence of morphologically disturbed systems (e.g., Conselice et al. 2003; Lotz et al. 2008b) and the frequency of optical pairs, either defined with respect to their relative velocity difference (e.g., Patton et al. 2002; Lin et al. 2004, 2008; de Ravel et al. 2008) or corrected for chance projections (e.g., Le Fèvre et al. 2000; Bell et al. 2006a; Kartaltepe et al. 2007). Parameterizing the redshift dependence as $\propto (1+z)^m$, the range of reported values is virtually unconstrained, with $m = 0-4$. Part of the problem may be the use of optical samples which we argued in previous work based on a near-IR sample (Bundy et al. 2004), may be biased by triggered SF (also see Berrier et al. 2006).

Although great care is needed in making comparisons with these methods, each of which defines a “merger” in a different way, it is now clear that there is considerable uncertainty in the literature regarding both the rate of merging and whether it rises substantially with redshift. Our goal in this paper is to overcome some of the problems faced in previous work by using a mass-limited sample of galaxy pairs drawn from the Great Observatories Origins Deep Survey fields (GOODS, Giavalisco et al. 2004). Our K_s -selected sample is more than 15 times larger than that discussed in Bundy et al. (2004). The enlarged sample allows us to identify pairs using the physically motivated definition of a major merger—as determined by the inferred mass ratio—and therefore enables us to measure the impact of mergers on mass assembly and make direct comparisons to evolutionary trends such as the formation rate of spheroidal galaxies. With our large sample size, we can study the merger rate as a function of mass, a key tool for testing the late assembly times predicted for massive galaxies. We can also distinguish dry and “wet” mergers (those involving significant cold gas reservoirs) as well as the types of galaxies most likely to host close companions. This project combines publicly available data in GOODS-S with new observations obtained in GOODS-N with the recently-commissioned Multi-Object Infrared Camera and Spectrograph (MOIRCS, Ichikawa et al. 2006) panoramic infrared imager on the Subaru 8.2m telescope.

Using this data set, we address two important ques-

tions in this paper. The first is whether the rate of major mergers since $z \sim 1$ is sufficient to explain the formation of new spheroidal and red-sequence galaxies over this redshift range. The second goal is to quantify the role of mergers in galaxy growth and determine whether the mass dependence of the merger rate is consistent with expectations based on hierarchical assembly.

A plan of the paper follows. In § 2 we introduce the new MOIRCS dataset and discuss its image processing and simulations undertaken to determine its limiting magnitude. We also present our analysis of complementary near-IR data that is publicly available and was obtained in GOODS-S using the Infrared Spectrometer and Array Camera (ISAAC) on the Very Large Telescope (VLT). The resulting K_s -band catalogs are correlated with a number of public redshift and imaging surveys, and the matched catalogs will be made available online. In § 3, we discuss our estimates of stellar masses, rest-frame colors, and morphologies. We present our methods for measuring pair fractions and comoving number densities in § 4. The results are described in § 5, while in § 6 we discuss the inferred merger rates and implications for both mass assembly and morphological/color transformations. A summary is provided in § 7.

Throughout this paper, we use the AB magnitude system and adopt a standard cosmology with $H_0=70$ h_{70} $\text{km s}^{-1} \text{Mpc}^{-1}$, $\Omega_M=0.3$ and $\Omega_\Lambda=0.7$.

2. DATA AND CATALOGS

Our study of galaxy pairs makes use of the GOODS fields, which not only provide deep HST imaging in four bands, but have also been targeted by many followup surveys at a variety of wavelengths. We begin this section with a description of the acquisition and reduction of our new MOIRCS data that delivers much-needed deep K_s -band coverage across the entire GOODS-N. We then turn to publicly available data, presenting first our analysis of near-IR imaging in GOODS-S obtained with ISAAC. These data are very similar in depth and resolution to the MOIRCS data, and together the two datasets provide the K_s -detected source lists that form the basis of the samples used in this paper.

We then discuss how we cross reference our K_s -selected catalogs to the many imaging and spectroscopic datasets that are available in both GOODS fields. Because a key part of our merger rate analysis uses redshift information to confirm potential galaxy pairs, it is important to make use of as many spectroscopic redshifts as possible. For this reason, we match our sample to the most up-to-date versions of available surveys including many of the recently completed ESO surveys in GOODS-S⁹. Finally, where previously measured spectroscopic or photometric redshifts are not available, we describe the additional photometric redshifts that are required to supplement our sample. Recognizing the value of K_s -selected multi-wavelength compilations in GOODS, the final matched catalogs will become publicly available at this website in early 2009: astro.berkeley.edu/~kbundy/KGOODS/

2.1. MOIRCS Near-IR Imaging

⁹ In GOODS-S, our catalog serves as a partial update to the MUSIC compilation of Grazian et al. (2006).

We obtained K_s -band observations using MOIRCS on the Subaru Telescope during two nights in April 2006. Each MOIRCS pointing is imaged onto two overlapping detectors, giving a total field of view that is roughly $4'$ by $7'$. Our observations consisted of 8 tiled pointings arranged with some overlap in order to cover the entire GOODS-N region. At each pointing, we executed three to four 9-point dither patterns (dithering by $15''$), coadding 4 exposures at each position. Individual exposure times varied from 50 to 55 seconds. The total integration time was typically one hour across the field with average seeing of $0''.5$. The MOIRCS K_s -band 80% completeness depth varies across the GOODS-N field from $K_s = 23.5$ to $K_s = 24.0$ with an average of $K_s \approx 23.8$.

We reduced the data using the MCSRED IRAF package written by Ichi Tanaka. Because MOIRCS is a relatively new instrument, we report in the Appendix on our modifications to MCSRED and solutions to other problems we encountered during the data reduction. Once the final images were reduced and combined we registered them to the GOODS-N ACS astrometry by comparing bright stars detected in both the MOIRCS and ACS data. Our Subaru observations were not taken in completely photometric conditions, and so photometric calibration was carried out by comparing to stars in the shallower ($K_s \lesssim 22.7$) Palomar K_s -band observations presented in Bundy et al. (2005).

We used SExtractor (Bertin & Arnouts 1996) to detect and measure the photometry of sources in each of our reduced images. Low signal-to-noise (S/N) borders were masked interactively and detections here were excluded. We used a DEBLEND_MINCONT value of 0.003, DETECT_MINAREA set to 8 pixels, and a convolution with a 3-pixel Gaussian filter. We experimented with the detection threshold, finding that a value of 1.2σ detected all potential sources in the data. Deblending is an obvious concern in close pair studies. We inspected many deblended sources, comparing them to their counterparts in the HST z -band imaging, and verified that the deblending algorithm successfully identifies what appears to be separate galaxies and not sub-components of individual systems. This problem is less extreme in our $0''.5$ seeing MOIRCS imaging—which smooths over fine sub-structure—than in the higher resolution HST data. Additionally, we mitigate the potential problem of over-deblending by setting a minimum to the pair separation ($r_{\text{sep}} > 5h^{-1}$ kpc) in the analysis that follows, although this has little effect on our results.

To investigate the completeness and photometric uncertainty of our data, we inserted numerous fake sources of varying magnitudes into the reduced images and then recovered them using the same SExtractor parameters that were applied to real sources. Fake sources were given Gaussian profiles with FWHM values similar to point sources. We define the image depth by the magnitude corresponding to a recovery rate of 80%. This depth implies a slightly lower detection rate (60–70%) for real galaxies, which are more extended (e.g., Conselice et al. 2007). The scatter in recovered magnitudes gives the photometric uncertainty as a function of magnitude.

2.2. ISAAC Near-IR Imaging

In GOODS-S, JHK_s imaging was obtained by an ESO/GOODS project¹⁰ using ISAAC on the VLT at the ESO Paranal Observatory. The survey details and data reduction are described in Retzlaff (in preparation). The final version 2.0 reduced and calibrated images are publicly available on the ESO website and, for the K_s -band are similar in quality to our MOIRCS data in GOODS-N. Covering GOODS-S required 26 pointings given ISAAC’s smaller field of view ($2.5'$ on a side). The K_s -band coverage amounts to 160 arcmin 2 with $\sim 95\%$ overlap of the GOODS-S ACS imaging. Images were also obtained in the J and H bands. After excluding low S/N image borders, small gaps ($< 1''$) separate a few of the ISAAC pointings. This is not ideal for companion searches, but has a negligible impact on our results. The K_s -band depth varies from 24.1 to 25.2 (AB) with seeing less than $0''.6$ on all images and typically more like $0''.5$.

As with the MOIRCS data, we used SExtractor to perform photometry on the ISAAC data in all three filters. We used a DEBLEND_MINCONT value of 0.0005, DETECT_MINAREA set to 8 pixels, and a convolution with a 3-pixel Gaussian filter. A combined source list was assembled with duplicates flagged in the same way as above. The image depth and photometric uncertainty was estimated using the same procedure of inserting fake sources. We note that these data were also used by Rawat et al. (2008) in a pair fraction study.

2.3. Matched Catalogs

We constructed our K_s -selected sample in GOODS-N by combining the detections in all of the MOIRCS images into a single source list. Because we designed the field layout so that the pointings overlap, duplicate sources must be removed from this list. We did this by searching for those sources that were within $1''$ of another source but were detected on a different MOIRCS image. The duplicate with the larger number of SExtractor warning flags (bad pixels, saturation, etc.) or worse photometric uncertainty was flagged and discarded from the analysis. The full GOODS-N K_s -band catalog contains 8112 unique sources over 164 arcmin 2 .

We matched this K_s -band source list to a number of publicly available catalogs in GOODS-N. Beginning with the HST data, we used the publicly available v1.1 GOODS-N z -selected ACS catalog¹¹ (Giavalisco et al. 2004). The search tolerance was $0''.5$ for $K_s > 22.8$ and $0''.7$ for $K_s < 22.8$ to account for possible centroiding problems for bright sources. Where the ACS and MOIRCS data fully overlap, $\approx 86\%$ of the K_s -band sources have an ACS counterpart. For sources with $K_s < 22.8$, this number increases to $\approx 98\%$.

We then cross referenced our K_s -band sample to several spectroscopic redshift catalogs. For the Team Keck Treasury Redshift Survey¹² (TKRS, Wirth et al. 2004), we adjusted the TKRS astrometry by $+0.37''$ in declination and used a search tolerance of $0''.6$ for $K_s > 22.8$ and $0''.7$ for $K_s < 22.8$. Of the 4364 TKRS matches we use the 1485 with secure redshifts designated by a “zquality” code of three or four. We use similar search criteria to match our source list to the publicly available compilations.

¹⁰ Program ID: LP168.A-0485

¹¹ <http://archive.stsci.edu/prepds/goods/>

¹² <http://tkserver.keck.hawaii.edu/tksurvey/>

tion of spectroscopic redshifts¹³ initiated by the survey work in Cowie et al. (2004), as well as the $1.4 < z < 3.0$ spectroscopic survey undertaken by Reddy et al. (2006). We also cross referenced our catalog with the spectroscopic redshifts obtained by Treu et al. (2005). Including TKRS, these comparisons provide a total of 2109 secure spectroscopic redshifts for the GOODS-N sample.

Finally, to obtain U -band observations in order to improve photo- z estimates, we cross referenced our catalog with the deep ground-based photometry obtained by the Hawaii Hubble Deep Field North Survey¹⁴ (HHDF-N, Capak et al. 2004). We downloaded the R -selected catalogs and adjusted the HHDF-N astrometry by $-0.^{\circ}1$ in RA and $+0.^{\circ}2$ in Dec to match the ACS-based astrometry used here. The search criteria were the same as for TKRS.

In GOODS-S, a source catalog based on the ISAAC data was constructed with the same methods used to build the MOIRCS catalog in GOODS-N. Matching to the v1.1 GOODS-S z -selected ACS catalog was also carried out in a similar fashion. The K_s -selected ISAAC catalog was correlated to source catalogs obtained from the ISAAC J and H -bands (JH photometry was not obtained in GOODS-N). The final ISAAC K_s -selected catalog in GOODS-S contains 9043 unique sources over 160 arcmin².

As with the MOIRCS-based catalog in GOODS-N, we matched the ISAAC catalog to several publicly available surveys. We downloaded Version 1.0 of the VIMOS GOODS/ADP Spectroscopic Survey¹⁵ (Popesso et al. 2008) and Version 3.0 of the FORS2 GOODS/ADP Spectroscopic Survey¹⁶ (Vanzella et al. 2008, and references therein), from the ESO/GOODS project website¹⁷. Matched photometry, several more spectroscopic redshift surveys, and high quality photo- z estimates are compiled in the GOODS-MUSIC sample (Grazian et al. 2006). We matched the VIMOS, FORS2, and MUSIC catalogs to our ISAAC K_s -selected catalog using a search tolerance of $0.^{\circ}6$. Only ESO redshifts with quality codes of A or B or MUSIC codes less than or equal to 1 (signifying high confidence in the given redshift) are used in our analysis. This provides 1683 secure spectroscopic redshifts for GOODS-S.

To summarize, our initial K_s -selected catalog, complete to $K_s \approx 23.8$, consists of 8112 sources in GOODS-N and 9043 in GOODS-S for a total of 17155. Of these, 14998 have ACS counterparts and 3792 have secure spectroscopic redshifts. In § 4 we build a mass-limited galaxy sample from these matched catalogs by imposing a magnitude cut of $K_s < 23.57$. The resulting sample forms the basis of our close pair analysis. Its properties are discussed in § 4.

2.4. Supplemental Photometric Redshifts

Redshifts are a key ingredient in this work. Not only are they necessary for examining how the pair fraction

evolves with time, but they are also used to reject chance projections and confirm true physical pairs. Unfortunately, spectroscopic redshifts are not always available and photometric redshifts are needed in both GOODS fields.

Previous photo- z estimates have been made by several authors, though not typically for K_s -selected samples. In GOODS-N, high quality estimates are available from the HHDF-N Survey, but these use ground-based multiwavelength images that are degraded to the worst seeing— $1.^{\circ}3$ in the U -band—in order to improve matched photometry which is performed in $3''$ diameter apertures. We found that faint companions with separations $r < 3''$ may not be detected or may have contaminated photometry in images with such poor seeing (Capak et al. 2004), and so we do not use the HHDF-N photo- z estimates in this paper.

Instead, for the 4703 sources (out of 6812 within ACS coverage) in GOODS-N without spectroscopic redshifts, we use the Bayesian Photometric Redshift code (BPZ) described in Benítez (2000). In GOODS-N, we include the U -band photometry when available from the HHDF-N survey combined with $2''$ diameter photometry in the ACS $BViz$ and MOIRCS K_s bands. Comparing to the spectroscopic redshifts available, photo- z outliers (defined by $|z_{\text{spec}} - z_{\text{phot}}| > 1$) account for 4% of the BPZ estimates, with $\sigma_{\Delta z/(1+z)} \approx 0.1$ once outliers are excluded.

In GOODS-S, photo- zs are required for 6636 sources out of the total 8319 sources within the ACS region. Precise photo- zs for 5196 were estimated using an ACS z -selected sample combined with careful PSF fitting and were released in the GOODS-MUSIC compilation. Excluding outliers, which account for a few percent, Grazian et al. (2006) obtain a photo- z precision of $\sigma_{\Delta z/(1+z)} \approx 0.03$. We use these high-quality photo- zs whenever possible in GOODS-S, but still require an additional 1440 photo- zs to provide redshifts for full GOODS-S catalog. We again use BPZ with U -band photometry from the MUSIC compilation combined with the ACS and JHK_s ISAAC photometry measured in $2''$ diameters. Comparing to spectroscopic redshifts in GOODS-S, we find an outlier fraction of the BPZ photo- zs of $\sim 10\%$ and $\sigma_{\Delta z/(1+z)} \approx 0.11$ with outliers excluded. This poorer performance of BPZ in GOODS-S compared to GOODS-N—despite the addition of the J and H bands—seems to result from the shallower U -band photometry in GOODS-S as well as a discrepancy in the ISAAC filter curves¹⁸.

In both fields comparisons to spectroscopic redshifts with $z \gtrsim 1.5$ revealed additional catastrophic photo- z failures (with incorrect estimates typically assigned to $z_{\text{BPZ}} \lesssim 0.5$). Without redshift comparisons at $z \gtrsim 1.5$, we would have overestimated our photo- z precision. It is worth emphasizing that judgments on the quality of photo- z estimates from any survey are limited by the nature of the spectroscopic comparison set that is available.

¹³ <http://www.ifa.hawaii.edu/~cowie/hhdf/acs.html>
¹⁴ <http://www.astro.caltech.edu/~capak/hdf>
¹⁵ Based on observations made with ESO Telescopes at the La Silla and Paranal Observatories under Program ID 171.A-3045.
¹⁶ Observations were carried out using the Very Large Telescope at the ESO Paranal Observatory under Program IDs: 170.A-0788, 074.A-0709, and 275.A-5060.
¹⁷ <http://www.eso.org/science/goods>
¹⁸ The ISAAC filter transmission curves released on the ISAAC instrument website (which give $K_{\text{AB}} - K_{\text{Vega}} = 1.761$) do not match the latest calibrations in the final Version 2.0 release. The documentation reports that the throughput has been remeasured for Version 2.0, giving $K_{\text{AB}} - K_{\text{Vega}} = 1.895$. Updated ISAAC transmission curves—an input to BPZ—have not been made available, however.

3. GALAXY PROPERTIES

The deep K_s -selected catalogs described above provide a powerful dataset for our galaxy pair analysis. Before describing the mass-limited sample we draw from this dataset and the methodology we use to study pairs, we present our techniques for estimating three key physical galaxy properties that allow us to characterize the role of merging among different galaxy types.

3.1. Stellar Masses

The first of these properties is the stellar mass (M_*), which is estimated using the Bayesian code described in Bundy et al. (2006). SED fitting is performed using the 2'' diameter $BVizK_s$ photometry and the best available redshift. The observed SED of each galaxy is compared to a grid of 13440 models from the Bruzual & Charlot (2003) population synthesis code that span a range of metallicities, star formation histories (parametrized as exponentials), ages, and dust content. No bursts are included in our models and only those models with ages (roughly) less than the cosmic age at each redshift are considered. We use a Chabrier IMF (Chabrier 2003) and assume a Hubble constant of $70 \text{ km s}^{-1} \text{ Mpc}^{-1}$.

At each grid point, the K_s -band M_*/L_K ratios, inferred M_* , and probability that the model matches the observed SED is stored. This probability is marginalized over the grid, giving the stellar mass probability distribution, the median of which is taken as the final estimate of M_* . The width of the distribution provides the uncertainty which is typically 0.1–0.2 dex. This is added in quadrature to the K_s -band magnitude uncertainty to determine the final error on M_* . Stellar mass estimates for galaxies with photo-zs also suffer from the uncertainty in luminosity distance introduced by the photo- z error and the possibility of catastrophically wrong redshift information (Bundy et al. 2005; Kitzbichler & White 2007). We will take both into account in the analysis that follows.

More broadly, any stellar mass estimate suffers potential systematic errors from uncertainties inherent in stellar population modeling and various required assumptions, such as the form of the IMF. Several papers have stressed the importance of treating thermally pulsating asymptotic giant branch stars (TP-AGBs, e.g., Maraston et al. 2006) an element that is missing in the Bruzual & Charlot (2003) models. The recent and thorough investigation of population synthesis modeling by Conroy et al. (2008), however, argues that M/L ratios estimated from Bruzual & Charlot (2003) are largely resistant to the uncertain contribution from TP-AGBs as well as other limitations of current models. Still, it is important to recognize that M_* estimates may be affected by unrecognized systematic uncertainties at the 0.1–0.2 dex level.

3.2. Rest-Frame Color

We use the inferred rest-frame color to roughly split our sample into blue, star-forming galaxies and red, quiescent ones (see Willmer et al. 2006). We use the ACS rest-frame ($B - i$) color, with k -corrections determined from the SED fit performed by our stellar mass estimator. For each galaxy, the color of every model galaxy in the grid is weighted by the probability that the model matches

the observed SED. The weighted colors are then summed over the grid to derive the probability distribution as a function of ($B - i$) color. As with M_* we take the median of the distribution as the final color estimate.

The ($B - i$) distribution across the sample is bimodal, as expected. We define red galaxies to be those redder than $B - i = 1.3$ (AB units) in this filter system. This threshold results in very similar red/blue distributions and number densities as those reported in Willmer et al. (2006) and Bundy et al. (2006) using data from the DEEP2 Redshift Survey. We note however that while a restframe color partition is easy to implement, it is still a blunt method for discriminating star-forming from passive galaxies. For example, contamination from dusty star-forming galaxies on the red sequence is at least $\sim 10\%$ (see Yan et al. 2006) and a comparison to morphological types (see below) for a subset of galaxies with $0.6 < z < 0.8$ and $M_\odot > 10^{10}$ shows that $\sim 12\%$ of blue galaxies are classified as spheroidal while $\sim 24\%$ of red galaxies are classified as disk-like.

3.3. Morphology

Galaxy morphology is the final property we consider and is important because morphological evolution may be driven in part by merging. Morphological classification in the GOODS fields was presented in Bundy et al. (2005) and is publicly available¹⁹. The classification was carried out visually to a magnitude limit of $z_{\text{AB}} = 22.5$ which increases the effective mass limit of subsamples split by morphology, as we discuss below. Each source was assigned one of the following morphological types: -2=star, -1=compact, 0=E, 1=E/S0, 2=S0, 3=Sab, 4=S, 5=Scd, 6=Irr, 7=Unclass, 8=Merger, 9=Fault. As in Bundy et al. (2005), we group these definitions into the broader categories of spheroidals (types 0–2), disks (types 3–5), and irregulars (types 6–8). Visual morphologies are available for 1369 sources in GOODS-N and 1200 in GOODS-S.

4. METHODS FOR COUNTING GALAXY PAIRS

In any study of galaxy mergers, it is important to distinguish major from minor mergers, since major mergers—typically defined to have mass ratios between 1:4 and 1:1—have the potential to radically affect its morphology and star formation (e.g., Naab & Burkert 2003). With many previous studies lacking near-IR data, however, pair samples comprised an unknown mix of mass ratios. In fact, pairs defined using an optical magnitude difference may lead to inflated pair counts from triggered SF (Bundy et al. 2004), an effect that may worsen at higher redshifts where the global SFR increases. Thus an important goal of this work is to use our K_s -selected sample to select only those pairs with stellar mass ratios consistent with major mergers.

We implement this requirement by selecting pairs with a magnitude difference²⁰ of $\Delta K_s \leq 1.5$. Using pairs where mass estimates are available for both members, we find that this magnitude criterion results in mass

¹⁹ http://www.astro.caltech.edu/GOODS_morphs

²⁰ Recognizing the assumptions inherent in estimating M_* , our decision to use the *observed* magnitude difference as opposed to the *inferred* mass difference is designed to facilitate future comparisons to our results.

ratios $M_{\text{companion}}/M_{\text{host}} \geq 1/4$ for $\sim 80\%$ of the pairs. This number is greater than $1/6$ for 90% . Pairs are only included if found within a projected annulus of $5h^{-1} \text{ kpc} < r_{\text{sep}} < 20h^{-1} \text{ kpc}$ determined by the redshift of the primary or “host” galaxy, given our assumed cosmology ($H_0=70 \text{ km s}^{-1} \text{ Mpc}^{-1}$, $\Omega_M=0.3$ and $\Omega_\Lambda=0.7$). We avoid double counting by identifying only those companions that are fainter than their host galaxy. In order to infer the true physical pair fraction, we use two methods to remove chance projections from the raw pair counts defined above. The first uses a correction based solely on the sky density of background sources while the second employs redshift information to identify pairs in 3D space.

Before describing these methods in detail, we begin with a description of our mass-limited sample of host galaxies. It is important that the sample be clearly defined because the definition of the pair fraction, f_{pair} , is determined with respect to such a sample. With our definition, the number of paired systems is $N_{\text{pair}} = f_{\text{pair}} N_{\text{gal}}$, where N_{gal} is the number of host galaxies. Note that this definition differs from that of other authors in that f_{pair} is not the fraction of galaxies located in pairs (often termed N_c) but instead reflects the potential number of mergers within a sample ($f_{\text{pair}} \approx N_c/2$). Finally, because our sample allows us to determine not only the fraction, but the comoving number density of close pairs, we also describe our technique for estimating that quantity in this section. Converting the observed pair fractions into merger rates requires additional and uncertain assumptions, and we save this topic for § 6.

4.1. The Host and Companion Galaxy Sample

One of the primary advantages of our dataset is that both host and companion galaxies are drawn from a well-understood, K_s -selected catalog that can be characterized in terms of mass completeness. Based on the different depths of our near-IR images, we optimize our sample by choosing a K_s -band magnitude limit of $K_s = 23.57$. All companions and host galaxies must be brighter than this limit. Because companions are defined to be no more than 1.5 magnitudes fainter in the K_s -band than their corresponding host galaxy, this effectively means that our host sample is limited to $K_s < 22.07$.

Throughout this paper we will adopt three redshift intervals: $0.4 < z < 0.7$, $0.7 < z < 0.9$, and $0.9 < z < 1.4$. Given the K_s -band limit imposed, the host sample is complete in each redshift bin for masses greater than $\log M_*/M_\odot = 9.6$, 10.1, and 10.4. The corresponding completeness limits for potential companion galaxies at these redshifts are $\log M_*/M_\odot = 9.0$, 9.5, and 9.8. When morphological samples are considered, an additional z -band magnitude limit of $z_{\text{AB}} < 22.5$ is effectively imposed since reliable morphologies are difficult to obtain at fainter magnitudes. This increases the mass completeness limits of host galaxies to $\log M_*/M_\odot = 10.3$, 10.6, and 11.2. Below these values, some hosts may not be included in the sample. We highlight the impact of these limits on our results as we present them. These stellar mass limits are estimated by considering the detection efficiency of redshifted SED templates of burst-like stellar populations with a formation redshift of $z_{\text{form}} = 5$. Because of their high M_*/L ratios, these models provide conservative and accurate mass limit estimates.

Since companions are defined by being near their host galaxy, the field geometry of the sample is also important. We define contiguous survey regions within both GOODS fields where the K_s -band detection limit is greater than 23.57 and the ACS tiles maximally overlap (we exclude the triangular, low-S/N perimeters of the GOODS footprint). All of the ISAAC images in GOODS-S meet this requirement, giving a search area of 147 arcmin². We exclude three of the 16 MOIRCS images in GOODS-N because they are shallower than $K_s = 23.57$. This gives a final area of 139 arcmin² in the northern field, or 286 arcmin² with both fields combined. Only host galaxies separated by a distance greater than r_{max} from the border of the defined region are included (this removes $\sim 3\%$ from the sample). Stars, as determined visually in the morphology catalog of Bundy et al. (2005) and also as identified spectroscopically, are removed. The final host sample includes 2994 primary galaxies, more than 60% of which have spectroscopic redshifts.

Unfortunately, spectroscopic redshifts are not always available for both the host galaxy and potential companions. We must therefore make statistical corrections that account for the contamination of the true *physical* pair fraction from close, line-of-sight projections. We describe the two approaches we adopt for this correction below.

4.2. Method I: Projected Field Correction

Our first method for correcting the raw pair counts is common in past studies at high redshift (e.g., Le Fèvre et al. 2000) and assumes no redshift information for fainter companions is available. We require only that potential companions be detected in the K_s -band and that they satisfy the criteria described above. The field contamination for each host galaxy is measured according to the K_s -band source density (i.e., number counts) observed in the defined survey region in the magnitude interval $K_{\text{host}} < K_{\text{companion}} < K_{\text{host}} + \Delta K$, with $\Delta K = 1.5$. Because of cosmic variance, it is important to make this measurement separately for the host sample in GOODS-N and GOODS-S. For a given host galaxy, the measured sky density of possible contaminants is multiplied by the area of the corresponding search annulus to determine the contamination rate per galaxy. This is then summed across the potential host sample to estimate the total number of field contaminants, N_{corr} . We estimate the number of true physical pairs by subtracting N_{corr} from the total number of potential companions fulfilling the search criteria described above. As discussed in detail in §5, this method identifies 242 pairs within our sample, ~ 160 of which are expected to be chance projections. Uncertainties are determined by adding the Poisson error from N_{corr} and from the total raw pair counts in quadrature. We expect an additional contribution from cosmic variance in the relatively small GOODS fields.

4.3. Method II: Probable Redshift Confirmation

The vast majority of faint companions identified in the K_s -band catalog are also detected in the ACS and ground-based optical imaging which means that photometric redshifts can be estimated for these sources. A sizable fraction of companions ($\sim 30\%$) also have spectroscopic redshifts. In our second pair counting method,

we use the redshift information available for faint near-by neighbors to find those that are likely to be physically associated with their brighter host. This amounts to an additional redshift constraint on the identification of companions. For both the potential hosts and companions we define a redshift uncertainty of $\sigma_z = 0.002$ for galaxies with spectroscopic redshifts, $\sigma_z = 0.08(1+z)$ for galaxies with photometric redshifts²¹, and an unbounded σ_z for the remaining few galaxies without optical detections and therefore with no redshift information. When the redshift difference satisfies $\Delta z^2 < \sigma_{z,host}^2 + \sigma_{z,companion}^2$, the pair is selected²² with this method.

Because of the large redshift uncertainty, some of the host-companion pairs defined by photometric redshifts will be close in projection but not physically associated. As in our first pair counting method, a contamination correction is needed although it will of course be smaller since most contaminants are already excluded by their discrepant redshifts. As in Kartaltepe et al. (2007), we determine this correction factor by randomizing the coordinate positions of all the sources in our catalog (but retaining all redshift and magnitude information). Any companions identified in the randomized data are clearly chance superpositions. Thus, by repeating this exercise for 100 randomized datasets, we can estimate the average contamination rate, its uncertainty, and the dependence of these quantities on M_* and pair type (see below). Note that in the limit that no redshift information is available for faint neighbors this approach is equivalent to the first method described above. However, for surveys that contain dense environments like galaxy clusters (GOODS is too small to sample such environments), this technique underestimates the needed correction because it does not account for the increased rate of chance projections in dense regions.

Finally, we note that the possibility of catastrophic errors in photo- z estimates will cause some true physical companions to be disregarded as chance projections. We can determine the importance of this effect by examining the quality of our various photo- z estimates (§ 2.4) and estimating the likely number of catastrophic photo- z failures that cause us to underestimate the true number of pairs in method II. Based on this analysis we correct all f_{pair} values derived from method II upwards by 1%. Using method II, we find 89 pairs, ~ 41 of which are expected to be chance projections.

4.4. Estimating Comoving Number Densities

One of the important quantities we wish to determine in this work is the comoving volumetric merger rate as a function of the stellar mass of the host galaxy. As we discuss in § 6, this “merger rate mass function” provides a powerful tool for understanding the role of galaxy mergers in driving mass assembly as well as evolution in the numbers of different populations such as ellipticals and red-sequence galaxies.

²¹ The value of $0.08(1+z)$ is somewhat arbitrary and represents a compromise between the BPZ photo- z uncertainty (~ 0.1) and the MUSIC photo- z uncertainty (~ 0.03).

²² For the pairs in our sample identified by method II, $\sim 26\%$ feature spectroscopic redshifts for both members, $\sim 39\%$ require at least one photo- z , $\sim 28\%$ require photo- zs for both members, and $\sim 7\%$ are without redshift information for the fainter companion

We estimate such mass functions using the simple V_{max} technique (Schmidt 1968). We weight host galaxies and associated pairs by the maximum volume in which they would be detected within the K_s -band limit in a given redshift interval. In practice, our magnitude limits impose restrictions only in the highest redshift bin ($0.9 < z < 1.4$). For each host galaxy i in the redshift interval j , the value of V_{max}^i is given by the minimum redshift at which the galaxy would drop out of the sample,

$$V_{\text{max}}^i = \int_{z_{\text{low}}}^{z_{\text{high}}} d\Omega \frac{dV}{dz} dz \quad (1)$$

where $d\Omega$ is the solid angle subtended by the survey area, and dV/dz is the comoving volume element. The redshift limits are given as,

$$z_{\text{high}} = \min(z_{\text{max}}^j, z_{K_{\text{lim}}}^j) \quad (2)$$

$$z_{\text{low}} = z_{\text{min}}^j \quad (3)$$

where the redshift interval, j , is defined by $[z_{\text{min}}^j, z_{\text{max}}^j]$ and $z_{K_{\text{lim}}}^j$ refers to the redshift at which the galaxy would still be detected below the K_s -band limit for that particular redshift interval. We use the best-fit SED template as determined by the stellar mass estimator to calculate $z_{K_{\text{lim}}}^j$, thereby accounting for the k -corrections necessary to compute V_{max} values (no evolutionary correction is applied).

5. RESULTS

5.1. The Stellar Mass Dependent Pair Fraction

As discussed in § 1, the hierarchical framework that underlies current galaxy formation models argues that the mass scale on which galaxies assemble increases with time. Observations of star formation quenching and morphological evolution show that these processes are set by a mass scale that decreases with time (downsizing). Meanwhile, galaxy mergers are thought to be key drivers of both hierarchical assembly and the evolution of SF and galaxy morphology. So, understanding the mass dependence of merging provides a critical test of the role mergers play in galaxy mass assembly and evolution.

We begin our investigation of how galaxy mergers depend on mass by presenting the pair fraction measured using the two methods described in the previous section. With method I, in which no redshift information for companion galaxies is used, 242 pairs are found, ~ 160 of which are expected to be chance projections. The method I pair fractions, partitioned by mass and redshift, are plotted in the top panel of Figure 1. With method II, which takes companion redshifts into account, 89 pairs are found, ~ 41 of which are expected projections. The resulting method II pair fractions are plotted in the bottom panel of 1. In both cases, pair fractions are plotted for three redshift intervals: $0.4 < z < 0.7$, $0.7 < z < 0.9$, and $0.9 < z < 1.4$. The full sample (X symbols) as well as the dependence on the mass of the host, as indicated by the differently sized circular symbols, is shown. All of the plotted points are complete in terms of stellar mass except for the highest redshift $10 < \log M_*/M_{\odot} < 10.5$ bin which is $\sim 80\%$ complete as a result of the K_s -band

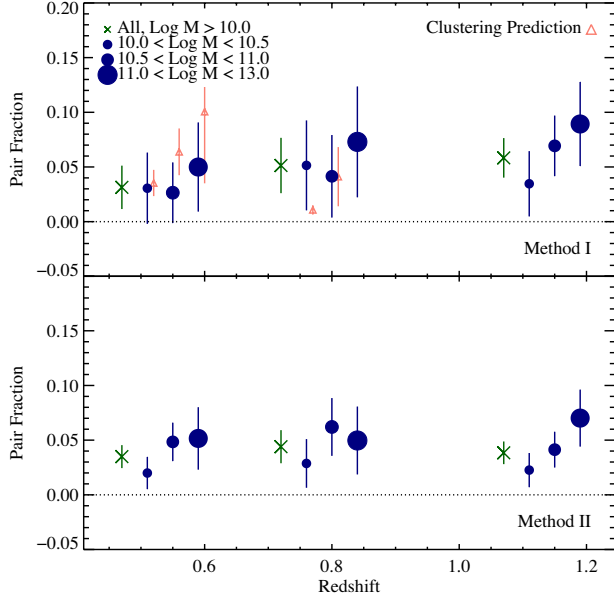


FIG. 1.— Contamination-corrected fraction of paired systems with $5h^{-1}$ kpc $< r_{\text{sep}} < 20h^{-1}$ kpc among galaxies in three redshift intervals. The top panel shows results determined using method I, the bottom panel method II. Abscissa values have been spaced to keep the data points from overlapping. The X symbols denote the full sample of primary (host) galaxies while the size of the circular symbols indicates the result of dividing these into stellar mass bins, as labeled. Predicted values of f_{pair} based on the 2-point correlation function (see § 6.1) of Zehavi et al. (2005) (using SDSS) are overplotted in the low- z bin of the top panel while the mid- z bin shows predictions based on Coil et al. (2006) (using DEEP2). The mass dependence of the clustering predictions is based roughly on the luminosity range probed by the clustering analyses.

limit. The results from both methods are listed in Table 1.

We first note that the two panels in Figure 1 are similar, reinforcing the utility of the two methods. Both plots show that roughly 2–5% of galaxies in a mass-limited sample host fainter companions. The value of f_{pair} depends on the maximum allowed pair separation, r_{max} . The average value of f_{pair} increases by an amount of 0.03 for $r_{\text{max}} = 25h^{-1}$ kpc compared to $r_{\text{max}} = 15h^{-1}$ kpc. This difference does not impact the derived merger rate because the expected merger efficiency decreases with larger r_{max} (e.g., Patton & Atfield 2008). We use $5h^{-1}$ kpc $< r_{\text{sep}} < 20h^{-1}$ kpc in what follows.

The key result in Figure 1 is the increase in f_{pair} among more massive host galaxies. Hints of this trend were observed by Xu et al. (2004) in their K -selected study of close pairs at $\langle z \rangle = 0.03$. We confirm it here with moderate significance to $z \gtrsim 1$ using both pair count correction methods. We verified that these results are still apparent for different values of r_{sep} including $r_{\text{sep}} = 15h^{-1}$ kpc and $r_{\text{sep}} = 25h^{-1}$ kpc. The mass dependence is also apparent in each GOODS field separately, suggesting that this trend is not a result of cosmic variance.

As we discuss in § 6, some of the increase at higher masses may reflect the stronger clustering of such galaxies. In that section, we return to the important question regarding the extent to which the mass dependence observed for the pair fraction translates into a mass dependence for the merger rate. Still, the fact that the

lowest mass bins in Figure 1 are nearly consistent with a zero pair fraction implies that the merger rate inferred from this and other studies is dominated by higher mass galaxies. We show in § 6.5 that this leads to the result that major mergers are unlikely to be the sole mechanism behind the formation of spheroidal galaxies and the red sequence. At the same time, the higher merger rates implied for massive galaxies shows that they are continuing to assemble after $z \sim 1$. This is an important piece of direct evidence for hierarchical growth which we seek to quantify in § 6.5.

Finally, we comment on the possibility that f_{pair} evolves with redshift. Averaging over the full mass range, $M_* > 10^{10} M_\odot$, we find no statistically significant evolution. With $f_{\text{pair}} \propto (1+z)^m$, we measure $m = 1.6 \pm 1.6$ using method I and $m = 0.3 \pm 1.4$ using method II.

5.2. The Dependence on Host Galaxy Color and Morphology

In addition to their role in mass assembly and their potential to affect the morphology and SFR of galaxies, mergers have also been invoked as a means to build the massive end of the red sequence. Successive dry mergers between early-type galaxies at lower masses can increase the numbers at higher masses (e.g., van Dokkum 2005; Faber et al. 2007). In this scenario, mergers must clearly be common within the red-sequence. We can begin to test this by characterizing the dependence of f_{pair} on host galaxy type. Our goal is not only to count the frequency of dry mergers, but also the remaining fraction of wet mergers since only these events can be responsible for morphological transformation or star formation quenching.

Both pair counting methods offer insight on the question of how the pair fraction varies with galaxy type. Since the first method relies on an entirely statistical field correction, we can only use it to study trends with host galaxy type. The properties of the companion and host together—the wet and dry merger frequency, for example—are accessible with method II and discussed below. Method I allows us to divide the host sample by both mass and type. Figure 2 shows the result when host galaxy type is defined using the color bimodality to separate star-forming from passive systems (also see Table 1). Bins corresponding to the most massive blue galaxies have not been plotted because they contain fewer than 10 hosts.

While the uncertainties have increased compared to Figure 1, there is weak evidence that the mass-dependent trend observed in Figure 1 is reflected in the star-forming properties of the host galaxies, with higher pair fractions found for quenched, red hosts, in large part because such galaxies dominate at the highest masses. This suggests a role for dry mergers in building the most massive early-type galaxies. However, a second interpretation discussed further in § 6 is that Figure 2 may reveal the greater degree of clustering among massive red galaxies. Finally, we note that the number of red hosts with companions in the lowest mass bin is consistent with zero. If confirmed with future studies, this observation would indicate that major mergers among red systems with $M_* \lesssim 10^{10} M_\odot$ cannot contribute significantly to the increasing abundance of red sequence galaxies at higher masses. Transforming blue galaxies into red objects via

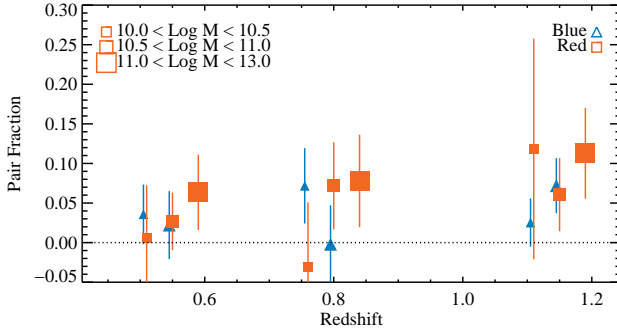


FIG. 2.— Color and mass dependence of the field-corrected pair fraction, f_{pair} using method I. The host sample has been divided into “blue” (blue triangles) and “red” (red squares) based on rest-frame color. Symbol size indicates stellar mass as in Figure 1. Bins corresponding to the most massive blue galaxies have not been plotted because they contain fewer than 10 hosts.

quenched star formation would therefore appear to be a more important mechanism for red sequence growth at $M_* \lesssim 10^{11} M_\odot$.

In Figure 3 we explore the relationship between pair fraction and galaxy morphology. Here the host sample has been restricted to $z_{\text{AB}} < 22.5$ which makes some mass bins incomplete (although we note we are measuring fractions not absolute quantities). Bins that are less than $\sim 80\%$ complete incomplete are indicated by lighter colors and open symbols and will tend to have an artificially lower number of redder galaxies. Given the large error bars, any trends observed here will require confirmation from larger studies. Still, there is a hint that spheroidals and irregulars host more companions than disk galaxies. Spheroidals, which are expected to be mostly red and quiescent, also tend to exhibit higher pair fractions among high-mass galaxies with $\log M_*/M_\odot > 10.5$ (although this is not the case at $z \sim 0.5$).

One intriguing and more robust result of Figure 3 is the appearance of a high fraction of irregular hosts at intermediate masses. In some ways, this is unexpected because irregulars represent only 10–20% of the galaxy population in our redshift range with $\log M_*/M_\odot \gtrsim 10$ (Brinchmann & Ellis 2000; Bundy et al. 2005; Pannella et al. 2006). They should therefore be less likely to host companions, if pairs were randomly distributed among all galaxy types. Even in incomplete bins which are biased against red spheroidals, host galaxies are more likely to have irregular morphologies than disk-like ones. Because we ignore companions with $r_{\text{sep}} < 5h^{-1}\text{kpc}$, the prevalence of irregular hosts tentatively suggests that even more distant companions can imprint significant morphological disturbances on their host galaxy, perhaps after executing a first pass (e.g., Lotz et al. 2008a). A similar conclusion was reached by Li et al. (2008) using SDSS. They also find an enhancement of SF among close pairs which could lead to morphological peculiarities. It stands to reason that not all irregular systems are in the last stages of a significant merger, which may in part explain why merger rates based on disturbed morphologies are typically higher than those inferred from pair counts (e.g., Conselice 2003; Lotz et al. 2008b).

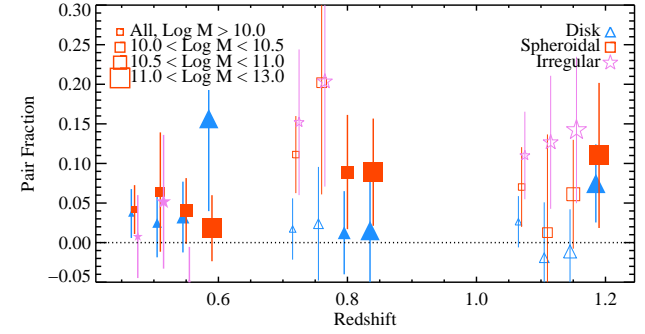


FIG. 3.— Morphological dependence of the field-corrected pair fraction using method I. The host sample has been restricted to $z_{\text{AB}} < 22.5$ and visually classified by ACS morphology into disks (blue triangles) and spheroidals (red squares) and irregulars (magenta stars). Symbol size indicates stellar mass as in Figure 1 with the smallest samples denoting the full mass range. Data points corresponding to bins that are significantly incomplete in stellar mass are indicated by lighter colors and open symbols.

Taken together, the type dependent pair fractions we have presented suggest that galaxies with higher masses, redder colors, and early-type morphologies tend to host companions more frequently than their lower mass, star-forming, and disk-like counterparts. This lends support to the concept of dry mergers as a mechanism for red sequence growth, especially at the highest masses, a point we return to in § 6.4. However, dry mergers do not appear to be important for building the red sequence at $M_* \sim 10^{10} M_\odot$ because the number of red hosts at these masses is nearly zero. At the same time, the enhanced pair fraction for more massive red and spheroidal galaxies may simply reflect the denser environments of these galaxies. The question of whether the derived merger rates are also enhanced in such environments is discussed in § 6.

5.3. The Frequency of “Dry” and “Wet” Pairs

In the top panel of Figure 4 we use method II combined with the rest-frame color of pair members to distinguish the fraction of pairs expected to result in dry and wet mergers (also see Table 2). Red-red pairs are identified as dry merger candidates. Blue-blue and mixed pairs indicate the presence of cold gas reservoirs and therefore represent potential wet mergers. For the few secondary (companion) galaxies without a redshift, the pair type cannot be determined and is labeled as “N/A.” Note that a statistical correction as described in § 4.3 has been subtracted from each category so that negative values are possible in some cases.

An interesting evolutionary signal appears in Figure 4. First, it appears that dry, red-red pairs are less frequent than their wet counterparts (the sum of blue-blue and mixed) in the highest redshift bin but become increasingly important with cosmic time, eventually dominating the low redshift bin. At the same time the number of blue-blue pairs decreases to zero. These trends are significant at the $1-\sigma$ level and may simply reflect the changing nature of the galaxy population with masses $\log M_*/M_\odot > 10.5$ which is increasingly dominated by red galaxies at late times. If our sample size allowed us to consider only high mass galaxies (e.g., $\log(M_*/M_\odot) > 11$) we might expect dry pairs

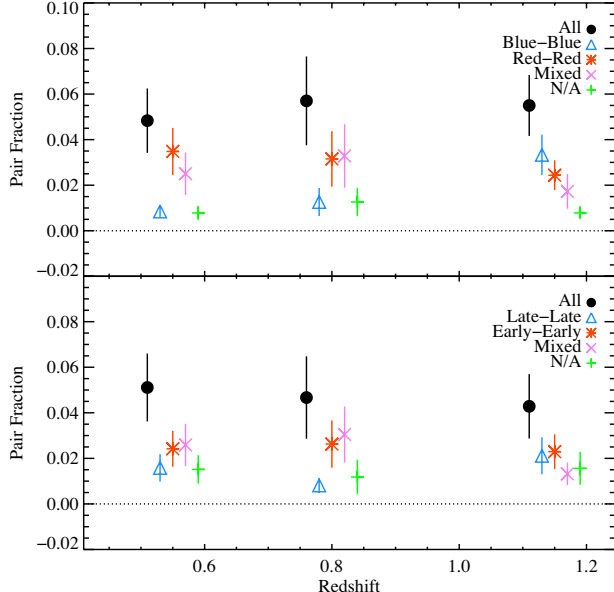


FIG. 4.— Fraction of dry, wet, and mixed pairs as defined by both color (top panel) and morphology (bottom panel), for host galaxies with $\log M_*/M_\odot > 10.5$. Pairs are confirmed using spectroscopic and photometric redshifts, and a correction for contamination and catastrophic photo-zs has been applied (method II). Pairs including secondaries without a redshift are listed as “N/A.” In the bottom panel, early-type refers to galaxies with spheroidal morphologies (E/S0/Sab) while late-type includes both disk-like and morphologically irregular galaxies. An additional magnitude cut of $z_{AB} < 22.5$ applies to the bottom panel.

among such galaxies to show an even earlier increase since this population evolves into quenched red galaxies first (Bundy et al. 2006; Borch et al. 2006; Bell et al. 2007). However, it is important to emphasize that the dry pair fraction is consistent with what is expected given the makeup of galaxies from which the pairs are drawn.

A similar conclusion was reached by Lin et al. (2008) who studied the fractions of blue-blue, red-red, and mixed systems among kinematic pairs identified in the DEEP2 survey. They also found a higher number of blue-blue pairs at $z \sim 1$ compared to the present day combined with an increasing number of red-red and, to a lesser extent, mixed systems. While that work benefits from spectroscopic redshifts for all pair members, our analysis has the advantage of being mass-limited and capable of selecting only major pairs. Furthermore, it does not require weighting to account for biases in the spectroscopic target selection. Given these very different but complementary methods, it is encouraging to see agreement both in the derived type-dependent pair fraction (note the different definitions of pair fraction: $f_{\text{pair}} = 0.5N_c$) and its evolution with redshift.

Our data also allow us to examine the frequency of pairs defined by the morphological type of both members. This is shown in the bottom panel of Figure 4 where it is important to remember that in the highest redshift bin, 30-40% of red galaxies with $\log(M_*/M_\odot) > 10.5$ will be missed because of the $z_{AB} < 22.5$ morphology cut. In this panel we label disk-like and irregular galaxies as “late-type” and spheroidals as “early-type.” We see no statistically significant trends, although there is a hint that late-late pairs are on par with early-early and mixed pairs in the highest redshift bin, but become sub-

TABLE 2
METHOD II: DRY, WET, AND MIXED MERGERS

Sample	z	N_P	N_{corr}	N_{gal}	$f_{\text{pair}} (\%)$
Color, $\log M_*/M_\odot > 10.5$					
Blue-Blue	0.4–0.7	4	2.3	514	1.3 ± 0.5
Blue-Blue	0.7–0.9	7	3.3	380	2.0 ± 0.8
Blue-Blue	0.9–1.4	24	9.4	793	2.8 ± 0.7
Red-Red	0.4–0.7	7	0.7	514	2.2 ± 0.5
Red-Red	0.7–0.9	5	0.9	380	2.1 ± 0.6
Red-Red	0.9–1.4	8	1.3	793	1.8 ± 0.4
Mixed	0.4–0.7	8	2.6	514	2.0 ± 0.6
Mixed	0.7–0.9	10	3.5	380	2.7 ± 1.0
Mixed	0.9–1.4	10	5.8	793	1.5 ± 0.5
N/A	0.4–0.7	0	1.1	514	0.8 ± 0.2
N/A	0.7–0.9	1	1.0	380	1.0 ± 0.4
N/A	0.9–1.4	1	1.2	793	1.0 ± 0.2
Morphology, $\log M_*/M_\odot > 10.5$					
Late-Late	0.4–0.7	2	1.5	482	1.1 ± 0.4
Late-Late	0.7–0.9	0	0.4	261	0.8 ± 0.3
Late-Late	0.9–1.4	3	0.5	322	1.8 ± 0.6
Early-Early	0.4–0.7	4	0.4	482	1.8 ± 0.4
Early-Early	0.7–0.9	3	0.2	261	2.1 ± 0.7
Early-Early	0.9–1.4	3	0.0	322	1.9 ± 0.5
Mixed	0.4–0.7	7	1.4	482	2.2 ± 0.6
Mixed	0.7–0.9	4	0.6	261	2.3 ± 0.8
Mixed	0.9–1.4	1	0.3	322	1.2 ± 0.4
N/A	0.4–0.7	4	1.5	482	1.5 ± 0.5
N/A	0.7–0.9	1	1.1	261	1.0 ± 0.6
N/A	0.9–1.4	2	0.9	322	1.3 ± 0.5

NOTE. — f_{pair} has been increased by 1% to account for losses due to catastrophic photo-z errors.

dominant in the mid- and low-z bins. Although larger datasets will be needed to confirm this, such an effect would be expected as the fraction of late-type galaxies declines with time.

As we discuss further in § 6, Figure 4 has important implications on the role of wet mergers in transforming blue (disk) galaxies into red (spherical) galaxies. Both indicate that the implied number of such wet mergers is a factor of ~ 2 less than the total merger rate. These figures also show that the rate of dry merging is not enhanced beyond what is expected given the makeup of galaxies in a mass-limited sample. In § 6 we show explicitly that neither morphological transformations occurring after wet mergers nor mass buildup caused by dry mergers appears sufficient to explain the increasing number of intermediate to very massive early-type galaxies.

5.4. Comparison to Previous Work

In this subsection, we discuss our results in the context of previous work. A number of close pair studies have been carried out using local surveys with $z \lesssim 0.3$ (e.g., Xu et al. 2004; De Propris et al. 2005; Masjedi et al. 2006; Patton & Atfield 2008). These tend to find very low pair fractions, often only a few percent. Using our full sample with $\log M_*/M_\odot > 10$, we find $f_{\text{pair}} = 0.03 \pm 0.02$ at $z \sim 0.5$. This is slightly above but consistent with the value of $f_{\text{pair}} \simeq 0.01$ reported by Patton & Atfield (2008) who analyzed a volume-limited r -selected SDSS sample (note that $f_{\text{pair}} \approx 0.5N_c$). They selected pairs with r -band luminosity ratios greater than 1/2 which is more stringent than our $\approx 1/4 M_*$ ratio

threshold and should lead to lower f_{pair} since not all major mergers are selected. Patton & Atfield (2008) find no luminosity dependence in their pair fraction estimate (with $r_{\text{sep}} = 5\text{--}20 h^{-1}$ kpc) in contrast to the mass dependence found here.

Xu et al. (2004) use the combination of the 2DFGRS and 2MASS surveys to measure both the fraction and number density of close pairs drawn from a K -selected sample at $\langle z \rangle = 0.03$. With a magnitude threshold of $\Delta K < 1$, their study is an excellent low- z analog to ours, and they estimate $f_{\text{pair}} \approx 0.02\text{--}0.03$ (their pair fraction is also defined as $2f_{\text{pair}}$) in good agreement with our lowest redshift bin. As mentioned previously, Xu et al. (2004) also find weak evidence for a higher value of f_{pair} for more massive galaxies. Our analysis confirms this finding and demonstrates that it continues to $z \sim 1$.

Studies at higher redshifts tend to focus on the evolution of the pair fraction with redshift as parametrized by m . This number is poorly constrained by recent work, with m varying from 0 to 4 (see Kartaltepe et al. 2007). Leaving evolution aside, better agreement in the average merger rate is being achieved, however. For example, our new results are consistent with the initial near-IR study undertaken by Bundy et al. (2004) and the work of Rawat et al. (2008) who perform a similar analysis using only spectroscopic redshifts in GOODS-S.

A number of optical studies of the pair fraction also deliver similar results, although some caution is needed in making comparisons. In addition to the bias in optical samples due to SF, our present work reveals a second effect. Depending on the selection method, optical samples may trace different stellar mass ranges as a function of redshift. Since we have shown that the pair fraction depends on M_* , this can bias the pair fraction at different redshifts. With this in mind, we note that the value of $f_{\text{pair}} = 0.02\text{--}0.03$ measured by both Bell et al. (2006a) using COMBO-17 as well as the kinematic pair study of Lin et al. (2004) and Lin et al. (2008) agrees with our findings here. Similar values were also found by Kartaltepe et al. (2007) and Hsieh et al. (2008) and, for $z \lesssim 0.8$, by de Ravel et al. (2008).

Not all merger studies find such low values, however. Our pair fraction is lower by a factor of 3–4 and shows less evolution compared to Le Fèvre et al. (2000), likely as a result of the SF bias. At the same time, morphological derivations of the merger fraction tend to find values of $f_{\text{pair}} \approx 0.1$ at $0.4 < z < 1.4$, 2–3 times higher than the results of our pair analysis (e.g., Conselice 2003; Lotz et al. 2008b). This may reflect the influence of non-uniform star formation, minor mergers, and even flybys on galaxy morphology as discussed with respect to Figure 3 (also see Lotz et al. 2008a).

6. DISCUSSION: THE GALAXY MERGER RATE

6.1. *Insight from Galaxy Clustering*

Our goal in measuring the pair fraction is to constrain the rate at which galaxies merge, but doing so requires knowing the fraction, C_{mg} , of close pairs that will eventually merge and on what timescale, T_{mg} , they coalesce. Both quantities are uncertain, but previous work has typically assumed that roughly half of close pairs will merge with a typical timescale of 0.5 Gyr (e.g., Patton et al. 2000). Under these assumptions, the pair fractions pre-

sented here would indicate that mergers occur more frequently among massive, red galaxies as compared to their less massive and bluer counterparts. But if either C_{mg} or T_{mg} depend on mass or galaxy type, this conclusion could be incorrect. As we now show, evidence from galaxy clustering may imply such a dependence.

The galaxy 2-point correlation function is typically measured on scales larger than $100 h^{-1}$ kpc and is usually fit as a power law $\xi = (r/r_0)^{-\gamma}$. By extrapolating this fit to the radii of interest for the close pairs in this paper, one can estimate the pair fraction predicted by clustering measurements made on larger scales. Assuming $\xi \gg 1$ and using our definition of f_{pair} ,

$$f_{\text{pair}} \approx 4\pi n_g \int_{r_{\text{min}}(1+z)}^{r_{\text{max}}(1+z)} r^2 \xi(r) dr, \quad (4)$$

$$= \frac{4\pi n_g}{3-\gamma} r_0^\gamma (1+z)^{3-\gamma} (r_{\text{max}}^{3-\gamma} - r_{\text{min}}^{3-\gamma}), \quad (5)$$

where n_g is the comoving galaxy number density of potential companions, and the $(1+z)$ factor accounts for the fact that r_{min} and r_{max} are defined in physical and not comoving coordinates.

We can use estimates of r_0 and γ from various clustering analyses to see how well the clustering signal extrapolated to small scales agrees with the pair fractions we measure. For example, Zehavi et al. (2005) measure luminosity dependent clustering in the SDSS. Taking their three brightest M_r luminosity bins to roughly correspond to our three stellar mass bins, we use $r_0 = 5.52, 6.16, 10.0$ in units of h^{-1} Mpc with $\gamma = 1.78, 1.85, 2.04$. We approximate n_g by integrating the mass functions of Bundy et al. (2006) and use $n_g = 4, 4, 0.8$ in units of 10^{-3} Mpc $^{-3}$ with $h = 0.7$. With these values and setting $z = 0.5$ (note that SDSS has an average $z \approx 0.1$), we find a predicted f_{pair} of 0.03, 0.06, and 0.10 for the three “mass” bins. These are overplotted in the first redshift bin of the top panel in Figure 1.

Extending this comparison to higher redshifts is difficult because the smaller sizes of high- z samples do not adequately probe the most massive or luminous galaxies. Still, we can compare to the $z \sim 1$ results of Coil et al. (2006) where we take $r_0 = 3.78 h^{-1}$ Mpc and $\gamma = 1.68$ from their median $M_B \approx -20.3$ sample 1 to correspond to our lowest mass bin ($\log M_*/M_\odot = 10\text{--}10.5$) and $r_0 = 4.21 h^{-1}$ Mpc with $\gamma = 1.9$ from their $M_B \approx -21$ sample 4 for our second mass bin ($\log M_*/M_\odot = 10.5\text{--}11$). We find $f_{\text{pair}} \approx 0.01$ and 0.04 and these results are plotted in the middle redshift bin of the top panel of Figure 1. It should be emphasized that M_B is not a good tracer of M_* and that the sample used by Coil et al. (2006) is not mass-limited (see Coil et al. 2008).

While the comparison between f_{pair} and predictions from the 2-point correlation function is clearly approximate, the resulting agreement is striking. Indeed, the lower correlation lengths of blue versus red galaxies (e.g., Coil et al. 2008) also seem to be consistent with the lower pair fraction of blue hosts shown in Figure 2.

This suggests that the connection between f_{pair} and clustering is a strong one and that the trends observed here may be expected given the way the correlation function increases with galaxy luminosity, stellar mass, and

TABLE 3
FRACTIONAL MERGER RATES, \mathcal{R}_{mg}

z	$\log M_*$ ($\log h_{70}^2 M_\odot$)	f_{pair} (Method I)	Patton & Atfield (2008)			Kitzbichler & White (2008)		
			C_{mg}	T_{mg} (Gyr)	\mathcal{R}_{mg} (Gyr $^{-1}$)	C_{mg}	T_{mg} (h_{70}^{-1} Gyr)	\mathcal{R}_{mg} (h_{70} Gyr $^{-1}$)
0.4 < z < 0.7	10.0 < $\log M_*$	0.03	0.58	0.5	0.036	1.0	2.0	0.016
0.7 < z < 0.9	10.0 < $\log M_*$	0.05	0.58	0.5	0.060	1.0	2.0	0.026
0.9 < z < 1.4	10.0 < $\log M_*$	0.06	0.58	0.5	0.068	1.0	2.0	0.029
0.4 < z < 0.7	10.0 < $\log M_*$ < 10.5	0.03	0.55	0.5	0.034	1.0	1.9	0.016
0.7 < z < 0.9	10.0 < $\log M_*$ < 10.5	0.05	0.55	0.5	0.057	1.0	1.9	0.027
0.9 < z < 1.4	10.0 < $\log M_*$ < 10.5	0.03	0.55	0.5	0.038	1.0	1.9	0.018
0.4 < z < 0.7	10.5 < $\log M_*$ < 11.0	0.03	0.58	0.5	0.031	1.0	1.4	0.019
0.7 < z < 0.9	10.5 < $\log M_*$ < 11.0	0.04	0.58	0.5	0.048	1.0	1.4	0.030
0.9 < z < 1.4	10.5 < $\log M_*$ < 11.0	0.07	0.58	0.5	0.080	1.0	1.4	0.050
0.4 < z < 0.7	11.0 < $\log M_*$	0.05	0.46	0.5	0.046	1.0	1.0	0.051
0.7 < z < 0.9	11.0 < $\log M_*$	0.07	0.46	0.5	0.067	1.0	1.0	0.075
0.9 < z < 1.4	11.0 < $\log M_*$	0.09	0.46	0.5	0.082	1.0	1.0	0.092

TABLE 4
VOLUMETRIC MERGER RATE MASS FUNCTION

Stellar Mass Range	0.4 < z < 0.7			0.7 < z < 0.9			0.9 < z < 1.4		
	$\log \Psi$	$\log \Psi_{\text{wet}}$	$\log \sigma$	$\log \Psi$	$\log \Psi_{\text{wet}}$	$\log \sigma$	$\log \Psi$	$\log \Psi_{\text{wet}}$	$\log \sigma$
10.0 < $\log M_*$ < 10.5	-3.77	-3.96	0.31	-3.69	-3.94	0.25	-4.16	-4.37	0.27
10.5 < $\log M_*$ < 11	-3.90	-4.09	0.29	-3.89	-4.14	0.26	-3.81	-4.03	0.13
$\log M_* > 11$	-4.51	-4.70	0.28	-4.38	-4.63	0.24	-4.50	-4.72	0.17
Volumetric Formation Rate of Spheroidals									
10.25 < $\log M_*$ < 10.55	-3.18	...	0.14	-3.12	...	0.09	-4.50	...	0.42
10.55 < $\log M_*$ < 10.85	-3.92	...	0.55	-2.91	...	0.08	-3.37	...	0.09
10.85 < $\log M_*$ < 11.15	-3.57	...	0.33	-3.02	...	0.10	-3.55	...	0.16
$\log M_* > 11.15$	-4.06	...	0.52	-3.44	...	0.17	-3.60	...	0.13

NOTE. — The values in this table are plotted in Figure 5. The symbol Ψ denotes a rate per unit volume (per logarithmic interval) with units of $h_{70}^{-3} \text{Mpc}^{-3} \text{dex}^{-1} \text{Gyr}^{-1}$. It should be distinguished from Φ , often used to represent mass or luminosity functions. Ψ_{wet} indicates the approximate volumetric merger rate after removing dry mergers. We use $\log \sigma$ to designate the associated statistical uncertainty (in dex). Stellar masses have units of $h_{70}^{-2} M_\odot$.

for red, early-type systems (e.g., Norberg et al. 2002; Zehavi et al. 2005; Li et al. 2006; Meneux et al. 2006; Coil et al. 2006, 2008; Meneux et al. 2008). In other words, the trends we observe with f_{pair} may be driven by regions of higher density which tend to host more massive, red-sequence systems.

6.2. Estimates of the Merger Timescale from Simulations

Perhaps the best way to estimate C_{mg} and T_{mg} is through detailed simulations. Unfortunately, fully numerical merger simulations are expensive and can only be performed for a handful of systems (e.g., Boylan-Kolchin et al. 2007). Cosmological simulations, meanwhile, are limited in resolution and require various analytic assumptions regarding dynamical friction, tidal interactions, and other details. Both Kitzbichler & White (2008) and Patton & Atfield (2008) use the Millennium Simulation to determine the fre-

quency and timescales of merging pairs, and after accounting for the fact that Kitzbichler & White (2008) absorb C_{mg} into their estimate of $\langle T_{\text{merge}} \rangle$ (see Patton & Atfield 2008), the two studies derive similar results on average.

Kitzbichler & White (2008) find that $\langle T_{\text{merge}} \rangle$ depends inversely on stellar mass as $M_*^{-0.3}$. This actually *enhances* the mass dependence of the merger rate beyond what we have observed for f_{pair} . In other words, the higher f_{pair} for massive galaxies translates into an even faster merger rate. Patton & Atfield (2008), on the other hand, assume that T_{mg} , defined for real-space pairs destined to merge, is a roughly constant 0.5 Gyr and instead investigate the dependence of C_{mg} (defined as f_{3D} in their paper) on luminosity. As might be expected from the Kitzbichler & White (2008) analysis, they find that C_{mg} increases with luminosity, resulting in more efficient merging for more luminous pairs (equivalent to a lower value of $\langle T_{\text{merge}} \rangle$ for more massive galaxies).

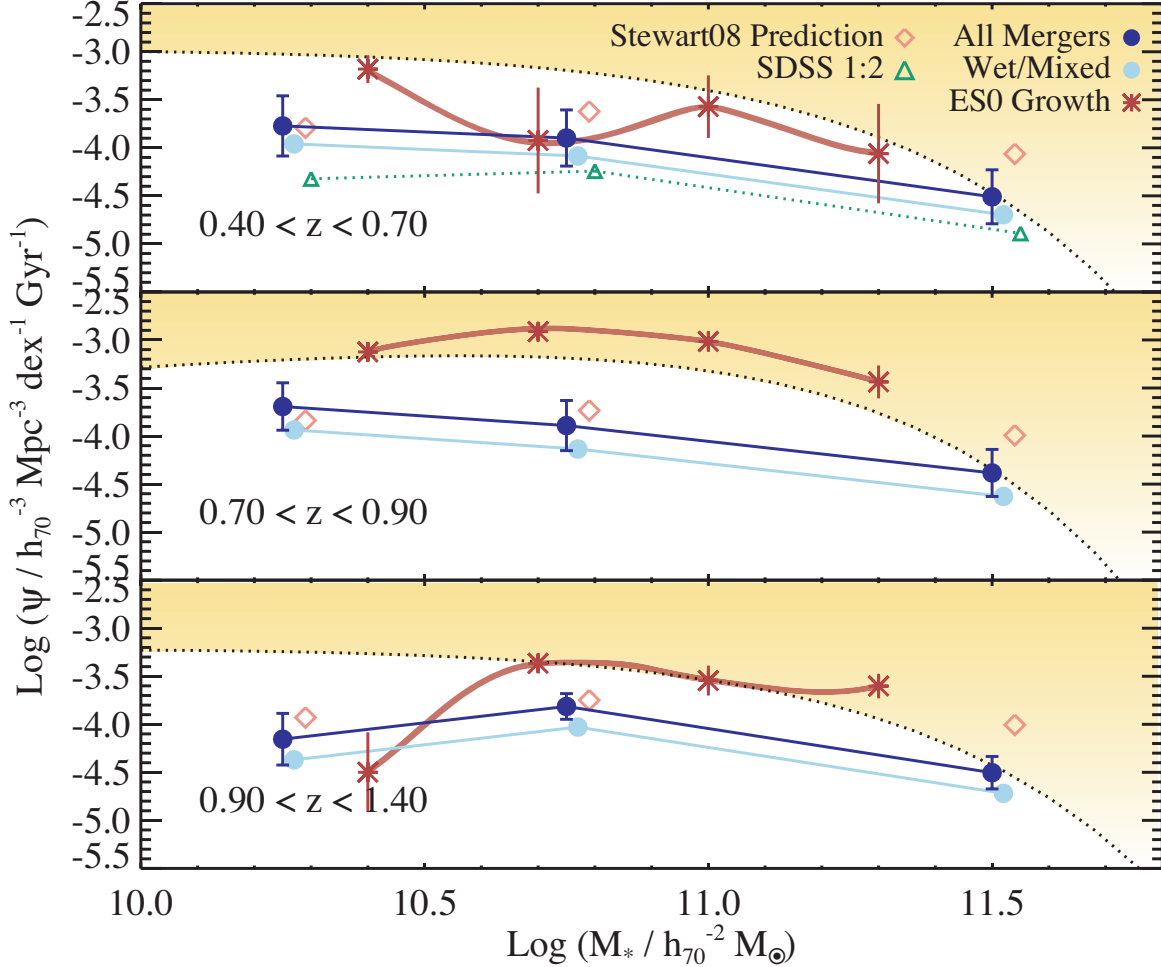


FIG. 5.— The major merger rate mass function in three redshift bins. The y-axis denotes Ψ , defined as a rate (per Gyr) per unit volume per logarithmic stellar mass interval. Solid circles indicate the observed merger rate for all galaxies determined with method I (see Fig 1) and assuming the values of T_{mg} and C_{mg} from Patton & Atfield (2008). Light blue circles show the result of excluding the approximate fraction of dry E/S0-E/S0 mergers, as measured in § 5.3. The green triangles in the first redshift bin reflect the luminosity-dependent volumetric merger rate at $z \sim 0.1$ computed for 1:2 or greater mass ratio mergers from the SDSS (Patton & Atfield 2008). Predictions for galaxy merger rates based on cosmological simulations from Stewart et al. (2008) are plotted as open diamonds. Red asterisk symbols show the rate of growth in the number of E/S0 galaxies based on the sample from Bundy et al. (2005). The rate of merging appears to be too low to fully account for the generation of new early-type galaxies. The dotted line in each panel indicates the average merger rate obtained if every galaxy experiences one merger over the range, $0.4 < z < 1.4$. Rates lying in the shaded region above these lines have a strong impact on the population, while those below have a minimal effect.

However, it is interesting that their most luminous pairs ($M_r \approx -22.8$ or $\log M_*/M_\odot \approx 11.2$) show a drop in C_{mg} which may be evidence of the clustering effect discussed above. The Patton & Atfield (2008) values therefore have a mild effect and translate the trend in f_{pair} into a slightly more moderate mass dependence for the merger rate.

6.3. The Merger Rate and Merger Rate Mass Function

Keeping in mind the substantial uncertainty involved with converting from f_{pair} to a merger rate, we derive merger rates using the assumptions in both Kitzbichler & White (2008) and Patton & Atfield (2008). In Table 3 we present the fractional galaxy merger rate, \mathcal{R}_{mg} , defined as $\mathcal{R}_{\text{mg}} \equiv C_{\text{mg}} f_{\text{pair}} / T_{\text{mg}}$. \mathcal{R}_{mg} can be thought of as the fraction of mergers per unit time within a sample of galaxies. We take the three most luminous bins in Patton & Atfield (2008) to correspond to

our three mass bins and use the fitting formula for T_{mg} (with C_{mg} set to 1.0) from Kitzbichler & White (2008).

With \mathcal{R}_{mg} determined, we use our mass-limited sample to self-consistently compute the volumetric merger rate (the number of mergers per unit time per unit comoving volume) as a function of the stellar mass of the primary or host galaxy. We call this the *merger rate mass function* and denote it using the variable, Ψ . The merger rate MF can be directly compared to differential evolution in the MFs of galaxies of various type, making it a valuable tool for evaluating the role of mergers in mass assembly and galaxy evolution.

The merger rate mass function is determined by multiplying the MF of the different host galaxy samples drawn from our survey (see 4.4) by the relevant value of \mathcal{R}_{mg} . In what follows, we use the values of \mathcal{R}_{mg} determined from the merger timescales and efficiencies reported by Patton & Atfield (2008) and listed in Table 3. Using the values from Kitzbichler & White (2008) leads to even

higher merger rates (by $\sim 10\%$) for the most massive galaxies. Our results are plotted as the dark solid circles in Figure 5. The error bars reflect the uncertainty in f_{pair} which dominates over the statistical uncertainty in the computed number densities. Both f_{pair} and the corresponding MFs have been determined using the same GOODS N+S dataset described in § 2. It should be emphasized, however, that both suffer from cosmic variance, although this problem is mitigated by combining two independent fields. We estimate that cosmic variance affects the data plotted in Figure 5 at the 0.2 dex level. The largest single source of uncertainty lies in the assumed values of T_{mg} and C_{mg} however.

The volumetric merger rate of the SDSS sample ($z \sim 0.1$) measured in different luminosity bins (with pair separation 5–20 h^{-1} kpc) by Patton & Atfield (2008) is roughly plotted as a function of mass in the low- z bin of Figure 5. Given the lack of strong redshift evolution in our sample, the lower merger rate from SDSS may simply reflect the fact that Patton & Atfield (2008) only consider merging pairs with an optical luminosity ratio greater than 1/2. Additional differences may arise in how C_{mg} and T_{mg} are applied to our different pair selection methods. Also shown in Figure 5 are predictions for the 1:4 or greater M_* ratio galaxy merger rate based on the cosmological N-body simulations and halo modeling performed in Stewart et al. (2008). These are multiplied by the observed MFs to derive the volumetric rates plotted. The agreement is remarkable, especially given the uncertainties in T_{mg} . There is a hint that the merger rate derived from observations falls below the model predictions, especially at the highest masses.

6.4. Hierarchical Mass Assembly Through Merging

Figure 5 provides key insight about the nature of galaxy mass assembly. The dotted line in the figure provides a benchmark useful for gauging the impact of mergers on the galaxy population at different masses. It is determined by dividing the galaxy abundance at each redshift (from the MFs of Bundy et al. 2006) by 4.5 Gyr, the amount of time spanning our redshift range, $0.4 < z < 1.4$. It is therefore the average event rate that would be obtained if every galaxy experienced exactly one merger over our redshift range. Rates that fall above this benchmark (in the shaded region of the plot) indicate a strong impact on the population. Rates that fall below correspond to processes with a minimal impact.

Figure 5 shows that for galaxies with $M_* \lesssim 10^{11} M_\odot$, the observed merger rate lies below our benchmark, indicating that major mergers have *not* contributed significantly to the assembly history of such galaxies since $z \sim 1$. For more massive galaxies the situation changes. In the highest mass bin, the merger rate is roughly on par with the benchmark rate, demonstrating that major mergers play a larger role in the recent assembly of such galaxies.

We can quantify this trend with the “merger remnant fraction,” that is the fraction of systems that have undergone major mergers in the different mass bins. This number is determined by integrating \mathcal{R}_{mg} over $0.4 < z < 1.4$. Using the results from method I, we find that at the highest masses, $\sim 30\%$ of galaxies experience a major merger. At the lowest masses probed, this number drops to 10–15%. These estimates are approximate because we

have not considered transfers across mass bins as a result of mergers and SF (see Drory & Alvarez 2008) and because of the large uncertainties in C_{mg} and T_{mg} (also see Bell et al. 2006b). Still, they reinforce the increasing importance of mergers on the assembly history of higher mass galaxies at $z \sim 1$.

Similarly, we can compare the volumetric merger rate to the average SFR measured as a function of M_* (e.g., Drory & Alvarez 2008). While measurements of $\text{SFR}(M_*)$ remain uncertain, this exercise indicates that the mass growth since $z \lesssim 1.5$ of galaxies with $\log M_*/M_\odot > 11$ is almost completely dominated by merging. For systems with $\log M_*/M_\odot \sim 10$, however, new growth from SF amounts to roughly 10 times the stellar mass accreted through major mergers, clearly indicating that SF is a far more important source of growth at lower masses. Considering the full mass range, $\log M_*/M_\odot \geq 10$, the mass accreted in major mergers over $0.4 < z < 1.4$ amounts to $\sim 15\%$ of the total stellar mass density of systems with $\log M_*/M_\odot \geq 10$ at $z \sim 0.8$. For $\log M_*/M_\odot \geq 11$, mass accretion through major mergers over the same redshift range accounts for $\sim 25\%$ of ρ_* at $z \sim 0.8$.

Qualitatively, our observations of an increase in the merger fraction with mass echo the hierarchical assembly of dark matter halos as determined with Λ CDM N-body simulations. In an analysis of the Millennium Simulation, Fakhouri & Ma (2008), for example, find that the *halo* merger rate (for halo mass ratios greater than 1:3) rises by $\sim 30\%$ from $M_{\text{DM}} = 10^{12}$ to 10^{13} . This mass dependence is significantly weaker but in the same sense as the factor of ~ 2 increase with mass we observe in the galaxy merger fraction among the $10 < \log M_*/M_\odot < 11.5$ galaxies thought to populate such halos.

The enhanced mass dependence in the galaxy merger rate may be due to the way halos are occupied (details forthcoming in Hopkins et al., in prep), specifically the inferred peak in the M_*/M_{DM} ratio at $M_{\text{DM}} \sim 10^{12} M_\odot$ (e.g., Wang et al. 2006; Mandelbaum et al. 2006) which roughly corresponds to the low-mass end of the range probed by our sample. In this scenario, the major merger rate of halos and galaxies should be directly related near the M_*/M_{DM} peak. But at higher masses M_* declines with respect to halo mass. This means that minor halo mergers can contribute to *major* galaxy mergers since less massive halos, being closer to the M_*/M_{DM} peak, have larger M_* fractions. Because there are always more minor than major halo mergers, this enhances the observed fraction of major galaxy mergers at higher masses. If our observations could probe below the peak, this interpretation would predict a suppressed galaxy major merger rate relative to the halo major merger rate since here some fraction of major halo mergers would host galaxies with a minor mass ratio.

Indeed, this qualitative picture is borne out in detail by Stewart et al. (2008). As discussed above, the galaxy major merger rate predicted from their model based on N-body simulations is in remarkable agreement with our observations (see Figure 5).

6.5. Are Spheroidals Formed in Major Mergers?

Another important insight gained from Figure 5 is the role of mergers in the formation of elliptical and red

sequence galaxies. The red asterisks in this plot show the formation rate (the rate at which the abundance increases) of visually classified spheroidal systems, as determined from the sample of Bundy et al. (2005). Error bars are Poissonian and do not include cosmic variance which we estimate enters at the ~ 0.2 dex level (see Stringer et al. 2008).

Figure 5 shows that the formation rate of new spheroidal galaxies is greater than the merger rate at nearly all masses and redshifts probed. The disagreement increases when only wet or mixed mergers are considered—only these can create new spheroidals. The light blue points show the merger rate mass function after the approximate fraction of dry spheroidal-spheroidal mergers (as measured in § 5.3) is subtracted. This result was anticipated by an analysis of the expected number of major halo mergers as measured in the Millennium Simulation which is also unable to account for the rate at which new spheroidals appear (Bundy et al. 2007; Genel et al. 2008). A similar conclusion applies to the inability of major mergers to account for the formation of red sequence galaxies which increase at a similar rate as the spheroidal population (e.g., Bell et al. 2007).

The discrepancy between major (wet) mergers and the formation of spheroidals shown in Figure 5 ranges from factors of ~ 3 –12. Simply interpreted, this requires mechanisms in addition to merging to make spheroids. How strong is this requirement? One concern is cosmic variance which could affect both the merger and spheroidal formation rates—we estimate the discrepancy could be overestimated by no more than a factor of ~ 2 as a result (Stringer et al. 2008). At the same time, the gap could be closed to some extent if the merger timescale were less than ≈ 0.5 Gyr (e.g., Lotz et al. 2008a). Indeed, a comparison of various theoretical treatments concludes that current predictions for T_{mg} are again uncertain at the factor of ~ 2 level (Hopkins et al., in prep.). Furthermore, our spheroidal classification, while dominated by ellipticals, includes S0’s and some Sa galaxies²³. The large bulges in such galaxies could be built in mergers with mass ratios less than 1:4, increasing the number of relevant mergers by $\sim 30\%$. Finally, multiple minor mergers can also drive morphological evolution. We would expect a factor of ~ 2 times more 1:10 minor mergers than the number of observed 1:4 mergers (e.g., Stewart et al. 2008). If ~ 3 such minor mergers have the equivalent morphological impact as one 1:4 merger (Bournaud et al. 2007; Hopkins et al. 2008), minor mergers can account for an additional $2/3 \approx 70\%$ of the morphological transformations needed to form spheroidals.

Assuming these potential systematic effects conspire in the same way and including minor mergers, it would be possible to reduce the discrepancy by a factor of ~ 6 . This would lend stronger support to the merger hypothesis and motivate a more precise treatment, but would still leave some tension at $z \sim 0.8$. For this reason and given the current observations and most recent theoretical assumptions, we conclude that other mechanisms in addition to merging may be needed to explain the transformation of disk-like galaxies into spheroidals (see

²³ The fact that it is so difficult to discriminate between such galaxies at $z \gtrsim 0.4$ is the reason we group them into a single “spheroidal” category (Brinchmann et al. 1998).

Parry et al. 2008) and the quenching of star formation.

7. SUMMARY

Using a deep K_s -selected catalog comprised of data from the GOODS fields, we have presented an analysis of the close pair fraction and implied merger rate of galaxies drawn from a mass-limited sample over the redshift range $0.4 < z < 1.4$. Using two methods of estimation, we find a relatively low pair fraction of $\sim 4\%$ with a redshift dependence of $(1+z)^{1.6 \pm 1.6}$. Our analysis strongly supports the basic conclusion of a low merger rate since $z \sim 1$, as deduced by several other recent surveys.

Our key observational finding is that the pair fraction of galaxies with $M_* > 10^{11} M_\odot$ is higher ($f_{\text{pair}} \sim 5$ –9%) than the corresponding pair fraction of lower mass systems ($f_{\text{pair}} \sim 2$ –4% for $M_* \sim 10^{10} M_\odot$). In addition, red systems and galaxies with spheroidal morphologies appear more likely to have companions than their blue or disk-like counterparts. This is in line with extrapolations of the correlation function to small scales. We find that the fraction of host galaxies classified as irregular (often more than half of hosts with $M_* < 3 \times 10^{10}$) is larger than the fraction of irregulars in the parent population (typically 10–20%). This supports the notion that orbiting companions can distort the primary galaxy even before a merger has occurred.

Dry mergers are only significant at the highest masses in our sample, $M_* > 10^{11} M_\odot$, but this appears to result from the fact that most galaxies in this mass range have already become red, early-type systems by $z \sim 1$. At lower masses ($M_* \sim 10^{10} M_\odot$) the fraction of red galaxies that host companions is consistent with zero, and we thus conclude that dry mergers alone are incapable of fully explaining the build-up of the red sequence, especially at $M_* \approx 2$ – $3 \times 10^{10} M_\odot$ where the formation of red galaxies is particularly rapid. In support of this conclusion, we also find that the number of dry pairs accounts for $\sim 50\%$ of all pairs in our mass range and evolves in way that is consistent with pairs drawn randomly from the parent population. The emerging picture is one in which dry mergers are not the main driver for red sequence growth but instead become increasingly common as a result of it.

By adopting estimates for the close pair merger efficiency and timescale, we determine the mass-dependent volumetric merger rate. From a comparison to the formation rate of galaxies with spheroidal morphology at the same redshifts, we conclude that the major merger rate is too low to fully explain the formation of spheroidal (and red sequence) galaxies since $z \sim 1$.

In terms of mass assembly, major mergers have a strong impact on galaxies with $M_* > 10^{11} M_\odot$, $\sim 30\%$ of which have experienced a major merger during the time spanning our redshift range. For less massive galaxies ($M_* \lesssim 3 \times 10^{10} M_\odot$), such mergers play a less significant role, affecting less than 10% of the population. For systems at such intermediate and lower masses, star formation is likely to be of much greater importance in driving growth. The higher merger fraction observed for the more massive galaxies in our sample provides direct support for hierarchical assembly and agrees with recent galaxy models based on N-body simulations, even if additional processes are required to explain the top-down nature of star formation downsizing and the formation

of spheroidal galaxies.

8. ACKNOWLEDGMENTS

We would like to thank Ichi Tanaka for his help in obtaining our Subaru observations and Yen-Ting Lin and Phil Hopkins for useful discussions. MF is supported by a Grant-in-Aid of the Ministry of Education of Japan. RSE acknowledges the financial support of the Royal Society.

APPENDIX

MOIRCS REDUCTIONS

We provide additional information on the MOIRCS data reduction, which was carried out using a modified version of the MCSRED package written by Ichi Tanaka. Simply using the package as written often led to the appearance of fringes across the entire reduced frame, especially for detector 2. More than half of our pointings were strongly affected, and the typical peak-to-trough fringe height was a few percent of the background level.

We traced the cause to two problems. First, strong fringing in one or two frames in an image set would be imprinted into other frames via the skyflat procedure and second, skyflats in MCSRED are made by averaging all images in a set. The flat field can vary over timescales of minutes, however, and changes (as well as the fringing) may be related to dithering the telescope. Thus a “running” sky flat that includes only some images taken before and after the science frame is desirable. We wrote a separate procedure which constructs running skyflats to flatfield the data and allows frames with bad fringing to be removed. The image registration portion of MCSRED also caused occasional problems, with some images being excluded from the final mosaic. By default, MCSRED calls the IRAF routine XYXYMATCH with the automated “triangles” registration option, which can sometimes fail for certain frames. When this happened we identified the positions of three stars common to all frames in an image set and supplied these to XYXYMATCH using the “tie points” method.

Careful inspection of the MOIRCS images revealed a curious pattern of noise spikes (although “noise worms” is a better description since they tend to be elongated) that often appear within $\sim 10''$ of bright sources (often stars) with $K_s \lesssim 16$. These objects are often detected as sources with $K_s \approx 23$ and, when they appear near galaxies, can be mistaken for fainter companions. We identified 133 such noise worms (about 1% of MOIRCS detections) and removed them from the photometric catalogs.

REFERENCES

Bell, E. F., Phleps, S., Somerville, R. S., Wolf, C., Borch, A., & Meisenheimer, K. 2006a, *ApJ*, 652, 270

Bell, E. F., Zheng, X. Z., Papovich, C., Borch, A., Wolf, C., & Meisenheimer, K. 2007, *ApJ*, 663, 834

Bell, E. F. et al. 2006b, *ApJ*, 640, 241

Benítez, N. 2000, *ApJ*, 536, 571

Berrier, J. C., Bullock, J. S., Barton, E. J., Guenther, H. D., Zentner, A. R., & Wechsler, R. H. 2006, *ApJ*, 652, 56

Bertin, E. & Arnouts, S. 1996, *A&AS*, 117, 393

Borch, A. et al. 2006, *A&A*, 453, 869

Bournaud, F., Jog, C. J., & Combes, F. 2007, *A&A*, 476, 1179

Bower, R. G. et al. 2006, *MNRAS*, 370, 645

Boylan-Kolchin, M., Ma, C.-P., & Quataert, E. 2007, *ArXiv e-prints*, 707

Brinchmann, J. & Ellis, R. S. 2000, *ApJ*, 536, L77

Brinchmann, J. et al. 1998, *ApJ*, 499, 112

Bruzual, G. & Charlot, S. 2003, *MNRAS*, 344, 1000

Bundy, K., Ellis, R. S., & Conselice, C. J. 2005, *ApJ*, 625, 621

Bundy, K., Fukugita, M., Ellis, R. S., Kodama, T., & Conselice, C. J. 2004, *ApJ*, 601, L123

Bundy, K., Treu, T., & Ellis, R. S. 2007, *ApJ*, 665, L5

Bundy, K. et al. 2006, *ApJ*, 651, 120

Capak, P. et al. 2004, *AJ*, 127, 180

Cattaneo, A., Dekel, A., Faber, S. M., & Guiderdoni, B. 2008, *preprint* (arXiv0801.1673), 801

Chabrier, G. 2003, *PASP*, 115, 763

Cimatti, A., Daddi, E., & Renzini, A. 2006, *A&A*, 453, L29

Cimatti, A. et al. 2004, *Nature*, 430, 184

Coil, A. L., Newman, J. A., Cooper, M. C., Davis, M., Faber, S. M., Koo, D. C., & Willmer, C. N. A. 2006, *ApJ*, 644, 671

Coil, A. L. et al. 2008, *ApJ*, 672, 153

Conroy, C., Gunn, J. E., & White, M. 2008, *ArXiv e-prints*

Conselice, C. J. 2003, *ApJS*, 147, 1

Conselice, C. J., Bershady, M. A., Dickinson, M., & Papovich, C. 2003, *AJ*, 126, 1183

Conselice, C. J. et al. 2007, *MNRAS*, 381, 962

Cowie, L. L. & Barger, A. J. 2008, *preprint* (arXiv0806.3457), 806

Cowie, L. L., Barger, A. J., Hu, E. M., Capak, P., & Songaila, A. 2004, *AJ*, 127, 3137

Croton, D. J. et al. 2006, *MNRAS*, 365, 11

De Lucia, G., Springel, V., White, S. D. M., Croton, D., & Kauffmann, G. 2006, *MNRAS*, 366, 499

De Propris, R., Liske, J., Driver, S. P., Allen, P. D., & Cross, N. J. G. 2005, *AJ*, 130, 1516

de Ravel, L. et al. 2008, *ArXiv e-prints*

Drory, N. & Alvarez, M. 2008, *ApJ*, 680, 41

Faber, S. M. et al. 2007, *ApJ*, 665, 265

Fakhouri, O. & Ma, C.-P. 2008, *MNRAS*, 386, 577

Genel, S. et al. 2008, *ApJ*, 688, 789

Giavalisco, M. et al. 2004, *ApJ*, 600, L93

Glazebrook, K. et al. 2004, *Nature*, 430, 181

Grazian, A. et al. 2006, *A&A*, 449, 951

Hopkins, P. F., Cox, T. J., Keres, D., & Hernquist, L. 2007, *preprint* (arXiv0706.1246), 706

Hopkins, P. F., Cox, T. J., Younger, J. D., & Hernquist, L. 2008, *preprint* (0806.1739)

Hsieh, B. C., Yee, H. K. C., Lin, H., Gladders, M. D., & Gilbank, D. G. 2008, *preprint* (arXiv0804.1604), 804

Ichikawa, T., Suzuki, R., Tokoku, C., Uchimoto, Y. K., Konishi, M., Yoshikawa, T., Yamada, T., Tanaka, I., Omata, K., & Nishimura, T. 2006, in *Proceedings of the SPIE*, Volume 6269, pp. 626916 (2006)., Vol. 6269

Juneau, S. et al. 2005, *ApJ*, 619, L135

Kartaltepe, J. S. et al. 2007, *ApJS*, 172, 320

Kitzbichler, M. G. & White, S. D. M. 2007, *MNRAS*, 376, 2

—. 2008, *preprint* (arXiv0804.1965), 804

Le Fèvre, O. et al. 2000, *MNRAS*, 311, 565

Li, C., Kauffmann, G., Heckman, T. M., Jing, Y. P., & White, S. D. M. 2008, *MNRAS*, 385, 1903

Li, C., Kauffmann, G., Jing, Y. P., White, S. D. M., Börner, G., & Cheng, F. Z. 2006, *MNRAS*, 368, 21

Lin, L. et al. 2004, *ApJ*, 617, L9

—. 2008, *ArXiv e-prints*, 802

Lotz, J. M., Jonsson, P., Cox, T. J., & Primack, J. R. 2008a, *preprint* (arXiv0805.1246), 805

Lotz, J. M. et al. 2008b, *ApJ*, 672, 177

Mandelbaum, R., Seljak, U., Kauffmann, G., Hirata, C. M., & Brinkmann, J. 2006, *MNRAS*, 368, 715

Maraston, C. et al. 2006, *ApJ*, 652, 85

Masjedi, M. et al. 2006, *ApJ*, 644, 54

Meneux, B. et al. 2006, *A&A*, 452, 387

—. 2008, *A&A*, 478, 299

Naab, T. & Burkert, A. 2003, *ApJ*, 597, 893

Norberg, P. et al. 2002, *MNRAS*, 332, 827

Pannella, M. et al. 2006, *ApJ*, 639, L1

Parry, O. H., Eke, V. R., & Frenk, C. S. 2008, *preprint* (arXiv0806.4189), 806

Patton, D. R. & Atfield, J. E. 2008, *preprint* (arXiv0806.0018), 806

Patton, D. R., Carlberg, R. G., Marzke, R. O., Pritchett, C. J., da Costa, L. N., & Pellegrini, P. S. 2000, *ApJ*, 536, 153

Patton, D. R. et al. 2002, *ApJ*, 565, 208

Popesso, P. et al. 2008, *preprint* (0802.2930), 802

Rawat, A., Hammer, F., Kembhavi, A. K., & Flores, H. 2008, *preprint* (0804.0078), 804

Reddy, N. A., Steidel, C. C., Erb, D. K., Shapley, A. E., & Pettini, M. 2006, *ApJ*, 653, 1004

Schmidt, M. 1968, *ApJ*, 151, 393

Stewart, K. R., Bullock, J. S., Barton, E. J., & Wechsler, R. H. 2008, *preprint* (0811.1218)

Stringer, M. J., Benson, A. J., Bundy, K., Ellis, R. S., & Quintin, E. L. 2008, *preprint* (arXiv0806.2232), 806

Toomre, A. 1977, in *Evolution of Galaxies and Stellar Populations*, 401–+

Treu, T., Ellis, R. S., Liao, T. X., & van Dokkum, P. G. 2005, *ApJ*, 622, L5

van Dokkum, P. G. 2005, *AJ*, 130, 2647

Vanzella, E. et al. 2008, *A&A*, 478, 83

Wang, L., Li, C., Kauffmann, G., & De Lucia, G. 2006, *MNRAS*, 371, 537

Willmer, C. N. A. et al. 2006, *ApJ*, 647, 853

Wirth, G. D. et al. 2004, *AJ*, 127, 3121

Xu, C. K., Sun, Y. C., & He, X. T. 2004, *ApJ*, 603, L73

Yan, R., Newman, J. A., Faber, S. M., Konidaris, N., Koo, D., & Davis, M. 2006, *ApJ*, 648, 281

Zehavi, I. et al. 2005, *ApJ*, 630, 1

TABLE 1
 RESULTS FOR f_{pair}

Sample	z	$\log M_*/M_{\odot} > 10$				$10 < \log M_*/M_{\odot} < 10.5$				$10.5 < \log M_*/M_{\odot} < 11$				$\log M_*/M_{\odot} > 11$			
		N_P	N_{corr}	N_{gal}	$f_{\text{pair}} (\%)$	N_P	N_{corr}	N_{gal}	$f_{\text{pair}} (\%)$	N_P	N_{corr}	N_{gal}	$f_{\text{pair}} (\%)$	N_P	N_{corr}	N_{gal}	$f_{\text{pair}} (\%)$
Method I																	
All	0.4–0.7	60	43.9	514	3 ± 2	37	29.4	250	3 ± 2	18	12.7	200	3 ± 2	5	1.8	64	5 ± 2
All	0.7–0.9	56	36.5	380	5 ± 3	33	23.6	183	5 ± 3	16	10.4	136	4 ± 3	7	2.6	61	7 ± 3
All	0.9–1.4	126	79.8	793	6 ± 2	53	41.7	326	3 ± 2	54	30.9	333	7 ± 2	19	7.1	133	9 ± 2
Blue	0.4–0.7	33	24.5	268	3 ± 3	27	20.0	183	4 ± 3	6	4.2	75	2 ± 3	0	0.3	10	-3 ± 3
Blue	0.7–0.9	33	21.9	212	5 ± 3	28	17.4	142	7 ± 3	4	4.0	58	0 ± 3	1	0.4	12	5 ± 3
Blue	0.9–1.4	87	59.2	574	5 ± 2	47	38.4	304	3 ± 2	33	17.8	206	7 ± 2	7	3.1	63	6 ± 2
Red	0.4–0.7	27	19.4	246	3 ± 3	10	9.4	67	1 ± 3	12	8.5	125	3 ± 3	5	1.5	54	6 ± 3
Red	0.7–0.9	23	14.6	168	5 ± 4	5	6.2	41	-3 ± 4	12	6.3	78	7 ± 4	6	2.2	49	8 ± 4
Red	0.9–1.4	39	20.5	219	8 ± 4	6	3.3	22	12 ± 4	21	13.1	127	6 ± 4	12	4.1	70	11 ± 4
Method II																	
All	0.4–0.7	21	8.2	514	3 ± 1	8	5.5	250	2 ± 1	10	2.3	200	5 ± 1	3	0.3	64	5 ± 1
All	0.7–0.9	23	10.1	380	4 ± 2	10	6.6	183	3 ± 2	10	2.9	136	6 ± 2	3	0.6	61	5 ± 2
All	0.9–1.4	45	22.5	793	4 ± 1	15	10.9	326	2 ± 1	20	9.6	333	4 ± 1	10	2.0	133	7 ± 1

NOTE. — We define N_P as the raw number of pairs, while N_{corr} is the estimated number of contaminants. The number of host galaxies is given by N_{gal} . Method II f_{pair} values have been corrected upward by 1% to account for catastrophic photo- z errors.